Tectonics

RESEARCH ARTICLE
10.1029/2019TC006051

Key Points:
- Central Qiangtang HP-bearing mélange formed by short-lived southward subduction in a divergent double subduction setting
- Progressive inversed shearing exhumed HP rocks
- Subduction reversal in a divergent double subduction zone can exhume HP rocks through direct slab movement

Supporting Information:
- Supporting Information S1
- Table S1
- Table S2
- Table S3
- Table S4
- Table S5

Correspondence to:
G. H. Wang, and P. D. Bons,
wgh@cugb.edu.cn;
paul.bons@uni-tuebingen.de

Citation:
Li, D., Wang, G. H., Bons, P. D., Zhao, Z. B., Du, J. X., Wang, S. L., et al. (2021). Subduction reversal in a divergent double subduction zone drives the exhumation of southern Qiangtang blueschist-bearing mélange, central Tibet. *Tectonics*, *40*, e2019TC006051. https://doi.org/10.1029/2019TC006051

Received 26 DEC 2019
Accepted 14 MAR 2020
Accepted article online 17 MAR 2020

[Correction added on 14 JAN 2021, after first online publication: Projekt Deal funding statement has been added.]

Subduction Reversal in a Divergent Double Subduction Zone Drives the Exhumation of Southern Qiangtang Blueschist-Bearing Mélange, Central Tibet

D. Li[1,2], G. H. Wang[1], P. D. Bons[1,3], Z. B. Zhao[4], J. X. Du[1], S. L. Wang[1], G. L. Yuan[1], X. Liang[1], L. Zhang[5], C. Li[1], D. R. Fang[6], Y. Tang[1], Y. L. Hu[1], and Y. Z. Fu[2]

[1]School of Earth Science and Resources, China University of Geosciences, Beijing, China, [2]Key Laboratory of Tectonic Controls on Mineralization and Hydrocarbon Accumulation of Ministry of Natural Resources, Chengdu University of Technology, Chengdu, China, [3]Department of Geosciences, Eberhard Karls University Tübingen, Tübingen, Germany, [4]Institute of Geology, Chinese Academy of Geological Sciences, Beijing, China, [5]Institute of Energy Sources, General Prospecting Institute of China National Administration of Coal Geology, Beijing, China, [6]Geoscience Documentation Center, China Geological Survey, Beijing, China

Abstract (Ultra) high-pressure (HP) rocks can be exhumed rapidly by subduction reversal or divergent plate motion. Recent studies show that subduction reversal can in particular occur in a divergent double subduction zone when the slab pull of one slab exceeds that of the other, shorter one, which then experiences a net upward pull. This recent hypothesis, first proposed for Triassic HP-rocks exposed in the central Qiangtang mélange belt in central Tibet, can explain the exhumation of (ultra) HP rocks through upward slab movement. However, this model lacks the support of kinematic evidence. In this study, based on the recognition of multiple deformational phases, we analyze the kinematics of the HP-bearing mélange in central Qiangtang. Based on new ^{40}Ar-^{39}Ar geochronology data and those collected from the literature, we present a temporal framework for the new observations. We recognize a switch in sense of shear between the prograde (D1) and exhumation (D2-3) paths. The change of shear sense reflects the reversal from downward to upward movement of the oceanic slab below. Early D2 represents the early exhumation stage that caused retrograde metamorphism from eclogite to blueschist facies. No magmatism occurred during this period. Continued exhumation from blueschist facies to greenschist facies resulted in D2-D3 structures. Voluminous igneous activity occurred during this stage. We suggest that subduction reversal in a divergent double subduction zone can best explain the kinematic evolution and temporal framework above. This exhumation model may provide a new perspective on the exhumation mechanism for other HP rocks around the world.

1. Introduction

The external parts of orogens are often linear, thick, and nonmetamorphic fold-and-thrust belts, whereas their interiors frequently expose exhumed high-pressure (HP) rocks (Chopin et al., 2012). Although pressure cannot be simply translated to depth (Li et al., 2010; Reuber et al., 2016;), the occurrence of these HP rocks is evidence that crustal materials can be tectonically transported to and exhumed from great depths of >100 km, well below the usual Moho depth (Erdman & Lee, 2014; Platt, 1993). However, compared with subduction that brings rocks down, the tectonic processes that carry deep-seated rocks back to the surface are less clear and still debated (Agard et al., 2009; Beaumont et al., 2009; Chopin, 2003; Ernst et al., 1997; Platt, 1993; Warren et al., 2008). It is generally accepted that the rapid burial of these rocks explains the low geothermal gradient (<800 °C at depths >100 km) (Hacker et al., 2013). Exhumation must probably also be rapid to preserve HP mineral assemblages in eclogites without significant retrogression (Brueckner & van Roermund, 2004) and is likely related to the subduction processes (Baldwin et al., 2004; Rubatto & Hermann, 2001).

A range of mechanisms has been proposed for the exhumation of HP rocks (Erdman & Lee, 2014; Guillot et al., 2009; Warren et al., 2008). These can be grouped in three broad classes, including (1) diapiric ascent of buoyant rocks (Little et al., 2011; Martinez et al., 2001), (2) wedge extrusion and/or subduction-channel flow driven by the pressure gradient and/or buoyancy forces within the wedge-shaped zone between subducting and overriding plate (Beaumont et al., 2001; Cloos, 1982; Gerya et al., 2002; Liao et al., 2018; Ring et al., 2010; Shreve & Cloos, 1986), (3) "eduction" or normal-sense upward motion of the whole

previously subducted slab as a coherent unit (Andersen et al., 1991; Brueckner & van Roermund, 2004; Duretz et al., 2012; Petersen & Buck, 2015). Most authors favor buoyancy of subducted continental slab as a driving force for eduction (Andersen et al., 1991; Chemenda et al., 1996), probably facilitated by slab breakoff (Duretz et al., 2011, 2012). However, Webb et al. (2008) and Brueckner and Cuthbert (2013) point out that extension may effectively pull the subducted slab up and away from underneath the overriding plate. This divergent motion of the formerly converging plates can be termed "subduction reversal (inversion)" (Webb et al., 2008), as it involves an inversion or reversal of the normally downward movement of the subducted slab. The inversion may, for example, be triggered by rotation of a microplate in a diachronous collision setting (Bottrill et al., 2014; Webb et al., 2008). Recently, Zhao et al. (2015) proposed that subduction reversal can also occur in a divergent double subduction configuration. In this hypothesis, subduction reversal occurs when the downward pull of the shorter oceanic slab is less than the opposing upward pull by the long subducting oceanic slab on the other side. HP rocks formed on the shorter slab are pulled out together with the short slab at plate tectonic rates. This model does not require particular circumstances such as microplate rotation or subduction of buoyant crust or even slab breakoff, and thus seems to be a relatively simple and efficient mechanism for the exhumation of (ultra) HP rocks.

This paper will revisit the HP rocks in the central Qiangtang mélange belt (CQMB) (Kapp et al., 2000; Li et al., 2006; Pullen & Kapp, 2014; Zhang et al., 2010) in central Tibet (Figure 1) for which Zhao et al. (2015) proposed subduction reversal to explain the Triassic exhumation of HP-rocks. The paper intends to show the importance of kinematic analyses to determine the directions of tectonic movements that need to be compatible with proposed subduction and exhumation scenarios.

2. Geologic Background

The Tibetan Plateau is an amalgamation of terranes or microcontinents that were accreted to the southern margin of Eurasia during the Phanerozoic (Kapp et al., 2003; Şengör, 1990; Zhang et al., 2004). From north to south, the interior of the Tibetan Plateau comprises the approximately east-west-trending Kunlun, Songpan-Ganzi, Qiangtang, and Lhasa terranes (Figure 1a). The Qiangtang terrane, separated from the Songpan-Ganzi complex to the north by the Paleo-Tethyan Jinsha suture, and from the Lhasa terrane to the south by the Mesotethyan Bangong-Nujiang suture (Zhang et al., 2007), represents a large part of the central Tibetan Plateau (Zhu et al., 2013). The Longmu Co-Shuanghu suture zone divides the Qiangtang terrane into the North Qiangtang (NQT) and South Qiangtang terrane (SQT) (Li et al., 2009; Zhai et al., 2011; Zhao et al., 2014, 2015) (Figure 1a). South of this suture, HP-rocks are found in the CQMB (Kapp et al., 2000, 2003; Pullen et al., 2010). This belt contains low-metamorphic grade pre-Permian basement rocks (Kapp et al., 2003; Liu et al., 2017; Zhang et al., 2013; Zhao et al., 2015), as well as a Triassic mélange with inclusions and rafts that range in size from cm to km. Inclusion lithologies are highly variable, including mafic rocks (ages range from 272 to 505 Ma; Wu et al., 2017; Zhai et al., 2013, 2016;), low-grade metasediments, including Permian limestones, as well as HP-rocks, mainly blueschists and eclogites (Kapp et al., 2000; Li, Zhai, Dong, & Huang, 2006; Pullen et al., 2010; Pullen & Kapp, 2014; Zhai et al., 2011; Zhang et al., 2006, 2010). The matrix of the mélange, however, appears of low-metamorphic grade at the most (Zhao et al., 2014, 2015). In places, the mélange is tectonically overlain by Late Paleozoic strata (Kapp et al., 2000, 2003; Pullen et al., 2010), while in other places the mélange is unconformably overlain by relatively undisturbed Late Triassic strata (Zhao et al., 2014, 2015).

Thermobarometry, U-Pb dating of zircons, and Lu-Hf dating of garnet indicate that the eclogites in the CQMB reached maximum pressures of 2.0–2.5 GPa at temperatures of 482–625 °C by ~240 Ma (244–230 Ma) (Kapp et al., 2003; Li, Zhai, Dong, & Huang, 2006; Pullen et al., 2008, 2010; Zhai et al., 2011; Zhang et al., 2006). Exhumation of the eclogites and blueschists occurred around 223–211 Ma (Dong et al., 2009; Kapp et al., 2003; Li et al., 2006; Li, Zhai, Dong, & Huang, 2006; Liang et al., 2012; Pullen et al., 2008; Zhai et al., 2009, 2011; Zhang et al., 2010). A stepwise exhumation was proposed based on a compilation of glaucophane and phengite Ar-Ar, and garnet Lu-Hf data (Liang et al., 2017). In the first exhumation stage, the eclogitic rocks were exhumed to blueschist conditions from ~240 (244–230) to ~225 Ma (227–223.4 Ma). The second exhumation stage, starting at ~225 Ma (233–220 Ma), brought these rocks to greenschist conditions generally after 222–217 Ma. Note that no magmatism (230–225 Ma) occurred during the early exhumation stage. Most of the igneous activity (225–209 Ma) (volcanic rocks; Fu et al., 2009, 2010; Li et al., 2007,

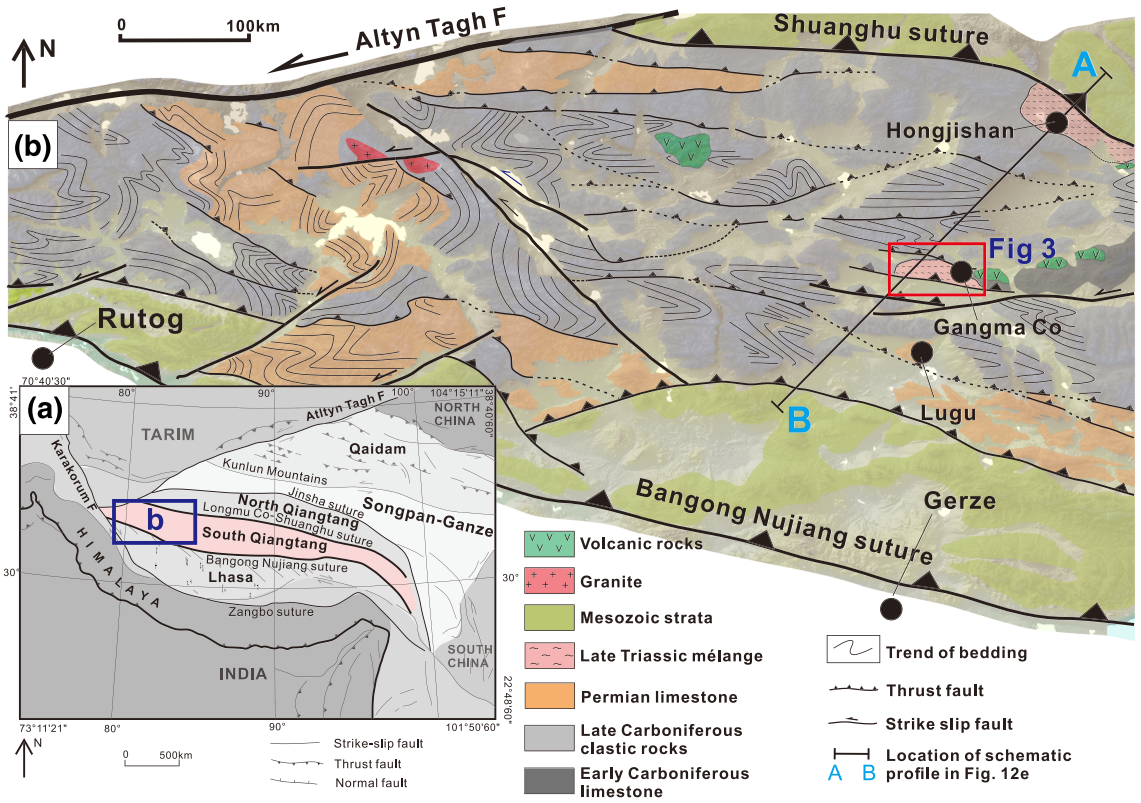

Figure 1. (a) Sketch of the main tectonic elements of Tibet. From north to south, the sutures are the Jinsha, Longmu Co-Shuanghu, Bangong-Nujiang, and YarlungZangbo suture zone. (b) Simplified geological map of the region (blue rectangle in (a)) around the study area (red rectangle) in the western part of the southern Qiangtang terrane, based on our mapping and interpretation of the 1:1,500,000 geological maps of the Qinghai–Xizang Plateau and adjacent areas Pan et al. (2004). The Shuanghu suture constitutes the northern boundary of southern Qiangtang terrane. These are cut by sinistral Atltyn Tagh Fault. The schematic cross section of Figure 12 is along the line AB.

2015, 2015; Wang et al., 2007, 2008; Zhai & Li, 2007; Zhai et al., 2013; Zhang et al., 2011; granite intrusions; Chen et al., 2014; Hu et al., 2010, 2010; Kapp et al., 2003; Liu et al., 2015; Wu et al., 2016; Zhai, Jahn, Wang, et al., 2013; Zhang et al., 2014) occurred during the second exhumation stage from blueschist to greenschist (Figure 2).

Several models have been put forward to explain the exhumation of HP-rocks in the CQMB. In the first, the "core complex model" of Kapp et al. (2000, 2003) and Pullen and Kapp (2014), the Qiangtang terrane is assumed to be a single terrane, never separated by an oceanic basin. The mélange is here supposed to have formed by low-angle, southward subduction of the Jinsha oceanic slab underneath the single Qiangtang terrane. Exhumation of the mélange in a metamorphic core complex-like dome subsequently resulted from slab rollback (Kapp et al., 2000; Pullen et al., 2010).

Most other authors favor models in which the SQT and NQT were separated since the Ordovician by the Longmu Co-Shuanghu ocean that finally closed in the Late Triassic (Li et al., 2009; Liang et al., 2017; Wang et al., 2017; Zhai et al., 2016; Zhang et al., 2010; Zhao et al., 2015). There is general agreement among these authors that this Paleo-Tethyan ocean subducted northward underneath the NQT (Li et al., 2009; Liang et al., 2017; Metcalfe, 2013; Zhang, Cai, et al., 2006; Zhang, Zhang, et al., 2006; Zhang et al., 2007; Zhao et al., 2014, 2015). Some authors (Zhao et al., 2015) invoke a second subduction zone where the oceanic slab subducted southward underneath the SQT, to form a divergent double subduction zone as described by Soesoo et al. (1997) for the Lachlan Fold Belt, SE Australia. In both cases, the mélange is supposed to have been thrusted southward upon collision of the SQT and NQT. In the single-subduction zone model, exhumation of the HP-rocks is assumed to have a occurred by extrusion from the subduction wedge (The wedge extrusion model; Liang et al., 2017; Zhang, Cai, et al., 2006, Zhang, Zhang, et al., 2006). Zhao et al. (2015) suggested that subduction mélange and HP-metamorphism developed on the southern subduction zone.

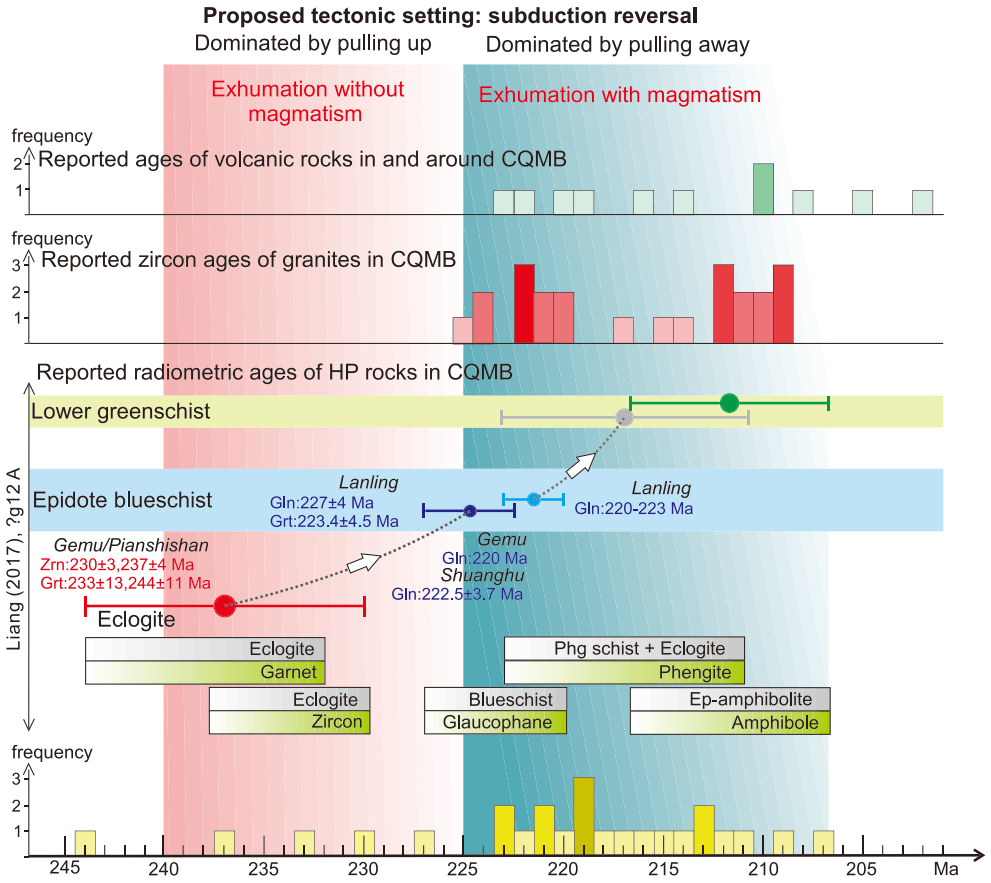

Figure 2. Compilation of published ages of metamorphism and igneous activity. Age data of volcanic rocks are from Li et al. (2007), Wang et al. (2007, 2008), Zhai and Li (2007), Fu et al. (2009, 2010), Zhang et al. (2011), Zhai, Jahn, Wang, et al. (2013), of granite rocks from Kapp et al. (2003), Hu, Cai, et al. (2010), Hu, Li, et al. (2010), Zhai, Jahn, Wang, et al. (2013), Chen et al. (2014), Zhang et al. (2014), Li, Li, et al. (2015, Li, Zhao, et al. (2015), Liu et al. (2015), Wu et al. (2016), and radiometric results of HP rocks in the central Qiangtang Metamorphic Belt Kapp et al. (2003), Li, Zhai, Chen, et al. (2006), Li, Zhai, Dong, and Huang (2006), Pullen et al. (2008), Dong et al. (2009), Zhai et al. (2009, 2011), Zhang et al. (2010), Liang et al. (2012). The inferred exhumation stages of the HP rocks come from Liang et al. (2017).

In their "subduction reversal model," Triassic reversal of the slab movement subsequently led to exhumation of these rocks. Upon closure of the oceanic basin, the two sutures merged into the single Longmu Co-Shuanghu suture zone. Collision resulted in southward thrusting of the mélange on top of the SQT.

A critical difference between the different models is the temporal evolution of shear direction in different parts of the system (Figure 3). The core-complex model predicts top-to-the-north shearing during progressive metamorphism toward eclogite facies conditions (Figure 3a). Both top-to-the-north and south could have occurred during exhumation by doming (Pullen et al., 2010). The wedge extrusion model with only northward subduction underneath NQT predicts top-to-the-south shearing during HP metamorphism and later overthrusting of the mélange on top of the SQT (Figure 3b). Sense of shear during exhumation would depend on the details of the extrusion model that led to the exhumation, but is usually also assumed dominantly top-to-the-south (Liang et al., 2017; Pullen & Kapp, 2014). Finally, the subduction-reversal model predicts top-to-the-north shearing during HP metamorphism, followed by top-to-the-south shearing and horizontal north-south extension during exhumation, and subsequent thrusting of the mélange on top of the SQT (Figure 3c). In all cases, the latest event is south-directed folding and thrusting related to the collision between the amalgamated Qiangtang terrane and the Lhasa terrane in approximately Early Cretaceous times (Zhao et al., 2017).

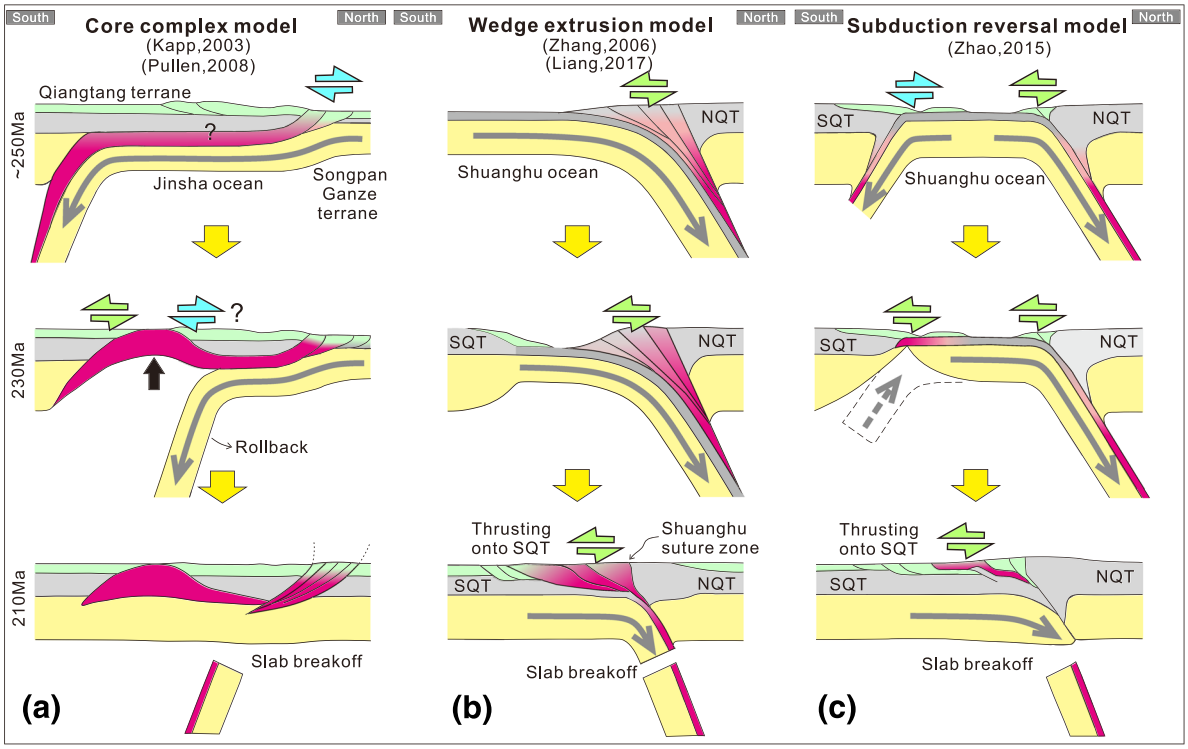

Figure 3. The three main published models for the exhumation of HP-rocks in the central Qiangtang Metamorphic Belt. (a) he "core-complex model." Top-to-the-north shearing is expected to occur during prograde metamorphism. Both top-to-the-north or south shearing may occur during the exhumation. (b) The "wedge extrusion model" in which top-to-the-south shearing is expected during the prograde metamorphism, exhumation, and later overthrusting. (c) The "subduction-reversal model." Top-to-the-north shearing should occur during prograde HP metamorphism, followed by top-to-the-south shearing and movement during exhumation and later thrusting.

The objective of this paper is to test the structural predictions of the current models by detailed kinematic and geochronology studies and to try to reconstruct the dynamic and tectonic evolution of the western part of the central Qiangtang HP-rock bearing mélange belt. Our results favor the model in which the HP-rocks were exhumed by subduction reversal in a double divergent subduction setting.

3. Geology of Gangma Co Area

We selected the Gangma Co area (Figure 1b) for 1:10,000 mapping to investigate the geology and deformation in the CQMB and surrounding units. The Gangma Co area is characterized by well-exposed mélange surrounded by Carboniferous-Permian strata (Kapp et al., 2003) (Figure 4).

3.1. Early Carboniferous Strata

Widely distributed nonmetamorphic fossiliferous limestones with intercalated fine-grained sandstone and siltstone layers are found in the center and SW of the study area. These are assigned to the early Carboniferous Riwanchaka formation, based on the typical Yangtze-type coral assemblage of *Guizhouphyllum* and *Yuanophyllum* (Liu et al., 2017).

Limestone breccias are found east of the mean outcrop area of the Riwanchaka formation, as well as at a few outcrops to its northwest. The matrix consists mainly of foliated limestone and mudstone, containing aggregates of limestone blocks (mainly 3–5 cm), some of which are foliated. These limestone breccias are always angular in shape and randomly distributed in the matrix. Occasional large blocks (up to 0.5 × 1.5 m) have clearly visible original bedding inside. Thinly layered cherts and fine-grained sandstones also often occur as blocks, and sometimes are folded and foliated. No obvious deformation, except for brecciation, is observed in the western outcrops of this breccia. Fossils were not found. The nature of this breccia, whether it is sedimentary or tectonic, remains enigmatic. Because of its proximity to the Riwanchaka formation outcrop area

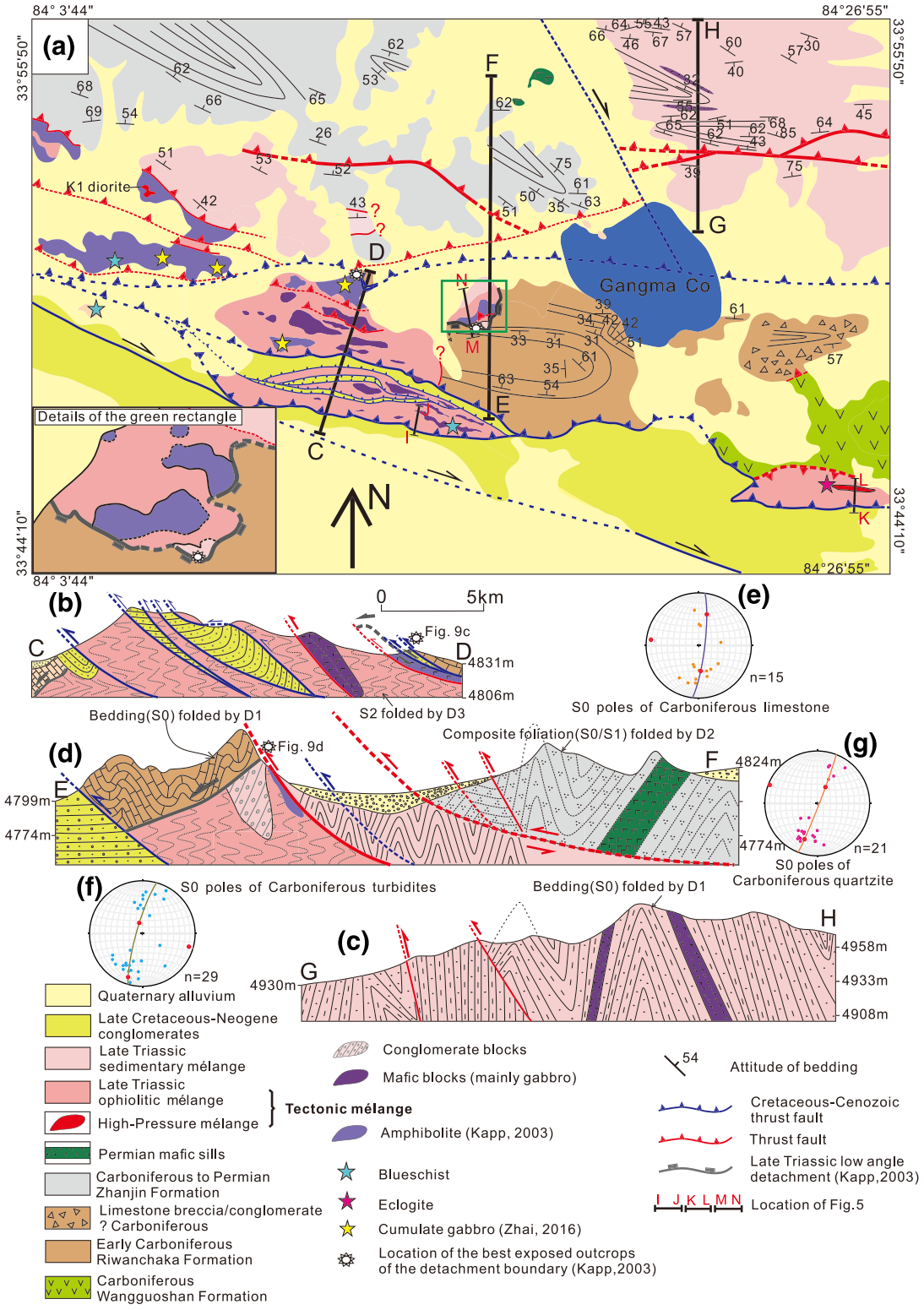

Figure 4. (a) Geological map of the Gangma Co area. This region contains mainly Carboniferous-Permian strata and chaotic mélange. Contacts of Carboniferous-Permian strata and mélange are modified from Kapp et al. (2003). Several south-vergent thrusts are identified, which place the mélange on top of Cretaceous-Cenozoic strata. Only the largest mafic blocks in the ophiolitic mélange are shown. The location of amphibolites or cumulate gabbro, blueschist, eclogites, and two best outcrops of the detachment (Kapp et al., 2003) are marked on the map. Panels (b)–(d) are cross section along the lines of C-D, E-F, G-H. Note that a cross section based on sections I-J, K-L, and M-N is shown in Figure 5. (e–g) Lower hemisphere, equal-area stereonets show measured attitudes of bedding in the Carboniferous strata and sedimentary mélange.

and its dominantly limestone composition, we tentatively assign it to the Riwanchaka formation, although we cannot exclude that (part of) it may belong to the sedimentary mélange described below.

3.2. Late Carboniferous to Permian Sediments and Magmatism

Late Carboniferous to early Permian strata of the Zhanjin formation in the NW of the study area consist of glaciomarine diamictites and quartzite with phyllite layers (Kapp et al., 2003; Liu et al., 2017). Large-scale cross bedding and parallel bedding structures can be observed in the quartzite (Li et al., 2018). Fossils are generally scarce in the Zhanjin formation except for the sporadically preserved Gondwana-type faunas of bivalve *Eurydesma* in the Rutog area which are assigned to a Late Asselian to Early Sakmarian age (Liu & Cui, 1983).

Widely distributed Middle Permian strata of the Longge formation composed mainly of limestone do not occur in the study area, but adjacent to it. The formation consists of gray limestones and massive, poorly bedded reefs. Fossils of coral constrain the age to the late Guadalupian (Zhang et al., 2013).

Volcanic rocks, mainly andesites, of the Wangguoshan formation are found in the east of the study area (Liu et al., 2017). The formation is supposed to be conformably overlain by the Riwanchaka formation (Dan et al., 2018; Liu et al., 2017). Zircon U-Pb dating results of the andesite are 351–346 Ma, suggesting a formation age in the early Carboniferous (Dan et al., 2018, 2019; Jiang et al., 2015). These rocks have been interpreted as an (oceanic) arc volcanics (Dan et al., 2018, 2019).

3.3. Gangma Co Mélange

Sedimentation was continuous from the Carboniferous into the Permian, but ceased at about 260 Ma (Zhang et al., 2012; Zhao et al., 2015), except for deposition of Gangma Co mélange of poorly constrained age. It mainly consists of ophiolitic mélange, HP mélange, and sedimentary mélange.

The ophiolitic mélange (Figure 4) is characterized by a matrix of strongly schistose or transposed mafic and metasedimentary rocks that surround weakly to moderately deformed but variably metamorphosed blocks of Carboniferous-Permian strata, mafic rocks, and minor epidote-blueschist facies mafic rocks (Kapp et al., 2003; Zhai et al., 2016; Zhang et al., 2007; Zhao et al., 2015). The juxtaposition of rocks of variable lithologies, deformation, and metamorphic grades is typical of a tectonic mélange (Cloos, 1982; Kapp et al., 2000). Most of the mélange matrix has a low, up to greenschist facies metamorphic grade. The same holds for the clasts. For example, deformed zones in quartzite blocks are sericite bearing and numerous metabasalt blocks experienced greenschist-facies metamorphism, but still preserve typical volcanic vesicular and amygdaloidal structures (Zhang, Cai, et al., 2006). This mélange with low-grade matrix and abundant greenschist facies blocks was already recognized and mapped by Kapp et al. (2003) as “greenschist unit” (“gsch”). However, our mapping significantly extends the outcrop area of this unit. Ophiolitic fragments such as serpentinite, gabbro, basalt, and minor plagiogranite (Zhai, Jahn, Su, et al., 2013; Zhai et al., 2016), some of which have experienced amphibole-facies metamorphism (Kapp et al., 2003), are widespread and commonly occur as isolated blocks within this unit. We thus assign this unit to the ophiolitic mélange of Zhao et al. (2015).

Previous studies have already noted that some blocks in the ophiolitic mélange are lithologically similar to rocks in the Upper Carboniferous-Permian strata (Kapp et al., 2003; Li, Zhai, Dong, & Huang, 2006; Li et al., 2018; Pullen et al., 2011; Zhang, Zhang, et al., 2006). For example, quartzite blocks in the mélange that show cross bedding and parallel bedding are similar to those in the Upper Carboniferous strata of Zhanjin formation. A weakly deformed marble block beneath the northward thrusted HP mélange (Figure 5) includes fossils of fusulinids that are similar to those found in the Middle Permian strata of Longge formation (Zhang et al., 2013). In addition, two coherent conglomerate blocks are observed in the ophiolitic mélange, and consist of rounded gravel clasts, mainly of quartzite, chert, diabase, granite, and graywacke, of varying size (<1 to >8 cm) in a partially altered matrix. The composition, roundness, and sorting of the conglomerate are very similar to those of the conglomerate blocks in the sedimentary mélange described below.

HP mélange occur as large rafts inside the ophiolitic mélange. For example, an East-West trending eclogitic unit exists as a south-dipping thrust sheet against the ophiolitic mélange in the SE of the study area (Figure 4). The eclogitic unit also shows a block-in-matrix structure. Foliations of the garnet phengite schist matrix wrap around a large coherent eclogitic block, abundant small eclogite pods, and quartzite blocks. The

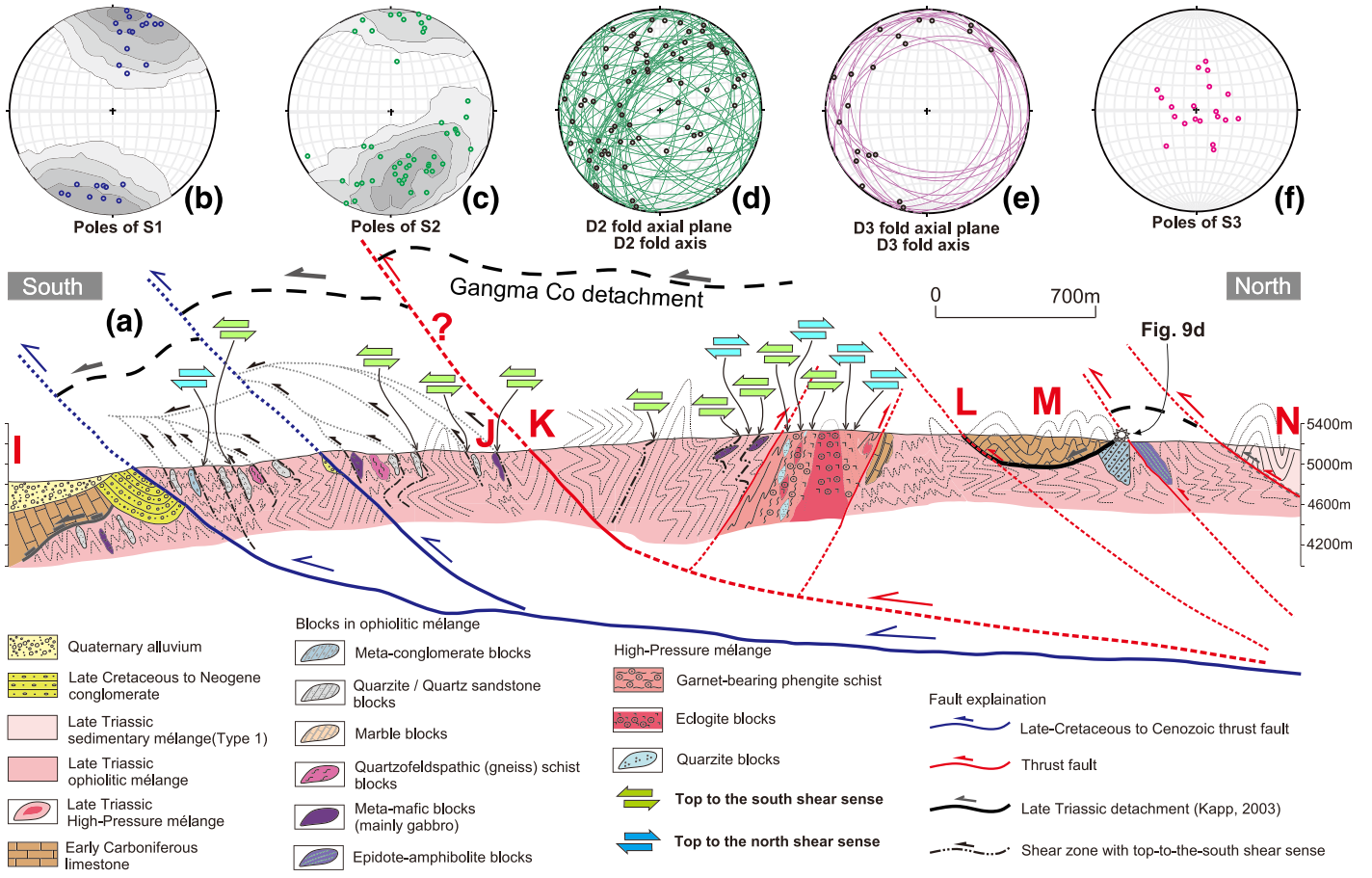

Figure 5. (a) Cross section of the Gangma Co mélange, compiled from sections I-J, K-L, and M-N on Figure 4a. The low-angle normal detachment fault between Carboniferous strata and mélange is modified from the cross section of Kapp et al. (2003). Dashed lines in the mélange represent the S1 foliation that is sheared and folded during later D2 deformation. D3 deformation in the cross section is characterized by shallowly dipping refolds of D2 shear zones, S2 foliation, and F2 folds. D4 north-dipping thrusts cut all the previous structures. The shear sense of D1 (blue) and D2 (green) structures as determined in the field and in thin section are shown. Mélange is placed onto Cretaceous-Cenozoic strata by a top-to-the-south thrust in the south. (b–f) Lower-hemisphere stereographic projection of poles of S1 to S3 foliations, as well as D2 and D3 axial planes and fold hinges.

core of the large coherent eclogite body is unfoliated, while the content and size of the garnet decrease toward its margin. Its outer margin consists of foliated amphibolite with rare garnets. The garnet phengite schist matrix has undergone eclogitic-facies metamorphism, as indicated by the inclusion of lawsonite pseudomorphs consisting of paragonite and zoisite in garnet. Because both the matrix and blocks have undergone eclogitic metamorphism, we assign this eclogitic unit into HP mélange.

Sedimentary mélange can be found in the NE of the area and west of Gangma Co (Figure 4). The matrix mainly comprises turbidites of fine-grained graywacke and siltstone. Grazing trace fossils can be found on the surface of the mudstones, implying a deep-water sedimentary environment. Sedimentary structures such as Bouma sequences and graded bedding are locally preserved. Individual matrix-supported conglomerates are up to ~1 m thick and contain rounded gravel clasts of quartzite, diabase, granite, and graywacke. Small limestone blocks poor in fossils and large limestone blocks with chert occur as lenses in the turbiditic matrix. In addition, Middle to Late Triassic (203, 237 Ma) mafic blocks (Gao et al., 2019) and debris flow deposits with Artinskian fusulines (Zhang et al., 2012) are reported in similar rocks in the Rongma area. This unit was also assigned to the greenschist unit by Kapp et al. (2003). However, this unit is nearly nonmetamorphosed as indicated by the preservation of fossils and primary sedimentary and microstructures. The mudstone is mainly metamorphosed into slate and phyllite with new minerals of sericite. Because of this and the strong similarity with the sedimentary mélange in Rongma area (Zhao et al., 2015), we reassign this unit to the sedimentary mélange.

3.4. Cretaceous to Neogene Sediments

Red strata (Figure 4) in the south of the study area consist of lower fluvial red clastics (Kapp et al., 2003) and unconformably overlying, poorly consolidated conglomerates, that have previously been assigned to the Neogene Kangtuo formation (Li et al., 2018). However, in the Rongma area and further south, bedding-parallel volcanic rocks near the base of the red strata were dated at 118–96 Ma (Zhao et al., 2017). Based on this, we assume that the earliest deposition time of the red strata in the study area may also be Cretaceous.

4. Geochronology

4.1. Methods

Rock samples for Ar/Ar dating (Figure 6) were crushed and then sieved. Mineral grains in fractions of ca. 250–380 μm were ultrasonically cleaned in distilled water. Muscovite grains were handpicked under a binocular microscope. The mica samples were then wrapped in aluminum foil, loaded into a tube of Al foil, and sealed into a quartz bottle. The bottle was irradiated for 24 hr in a nuclear reactor (Chinese Institute of Atomic Energy, Beijing). Gas purification was performed with Zr-Al getters. Ar isotope analysis was conducted on an Argus VI mass spectrometer at the Beijing Research Institute of Uranium Geology. All the measured isotopic ratios were corrected for mass discrimination, atmospheric Ar component, procedural blanks, and mass interference induced by irradiation. The correction factors of interfering isotopes produced during the irradiation were determined by the analysis of irradiated K_2SO_4 and CaF_2 pure salts. The values for the reactor correction factors were $(^{36}Ar/^{37}Ar)_{Ca}$ = 0.000278, $(^{39}Ar/^{37}Ar)_{Ca}$ = 0.000852, and $(^{40}Ar/^{39}Ar)_{K}$ = 0.001147. The standard samples were GBW04418 amphibolite, which has an age of 2,060 ± 8 Ma, a potassium content of 0.729 ± 0.005%, and an argon content of 109.06×10^{-6} (CCSTP/g), and ZBH-25 biotite, which has an age of 2,060 ± 8 Ma, a potassium content of 7.599%, and an argon content of 1.8157×10^{-9} (mol/g). The uncertainties on the apparent ages for each step are quoted at the 1σ level but weighted mean plateau ages and isochron ages are given at the 2σ level.

4.2. Results

Sample PM005-B20 is a medium-grained quartz mica schist, collected in the matrix of the HP mélange (Figures 6a and 6b). Muscovite from this sample yields an age plateau with a weighted mean of 212.9 ± 1.1 Ma defined by 82.09% of the total ^{39}Ar release (Figure 6c).

Sample PM005-B08 is a coarse-grained garnet-bearing quartz mica schist from the matrix surrounding eclogite blocks in the HP mélange (Figures 6e and 6f). Muscovite from this sample yields an age plateau with a weighted mean of 210.7 ± 1.4 Ma (MSWD = 6.5) defined by 95.63% of the total ^{39}Ar release (Figure 6g).

Both plateau ages are nearly identical to the isochron ages (Figures 6d and 6h).

5. Deformation History

Although there are abundant data on stratigraphy and metamorphism in the research area, only a few structural studies on the Gangma Co area have been published to date (Kapp et al., 2000, 2003). The Gangma Co ophiolitic mélange and its internal HP mélange raft have the characteristics of a tectonic mélange, and both have undergone a similar deformation history. Therefore, we present their deformation phases and kinematic data and analyses as a unified tectonic mélange below.

5.1. Deformation Only Found Within the Tectonic Mélange

Using overprinting relationships of deformation structures in outcrops and thin sections, we recognize four successive deformation stages (D1 to D4) in Gangma Co tectonic mélange. For clarity, structural data and descriptions are collected and organized as follows:

1. Representative pictures and descriptions of the deformation in the mélange were all obtained from the combination of measured geological sections I–N in the Gangma Co area (Figure 5) (including I–J, K–L, and M–N; Figure 4), to obtain one single, coherent image of the deformation structures. The organization of the pictures follows the successive deformation stages defined in this chapter.
2. The location of the detachment and south-vergent thrusts and folds are mainly illustrated on the Gangma Co geological map (Figure 4).

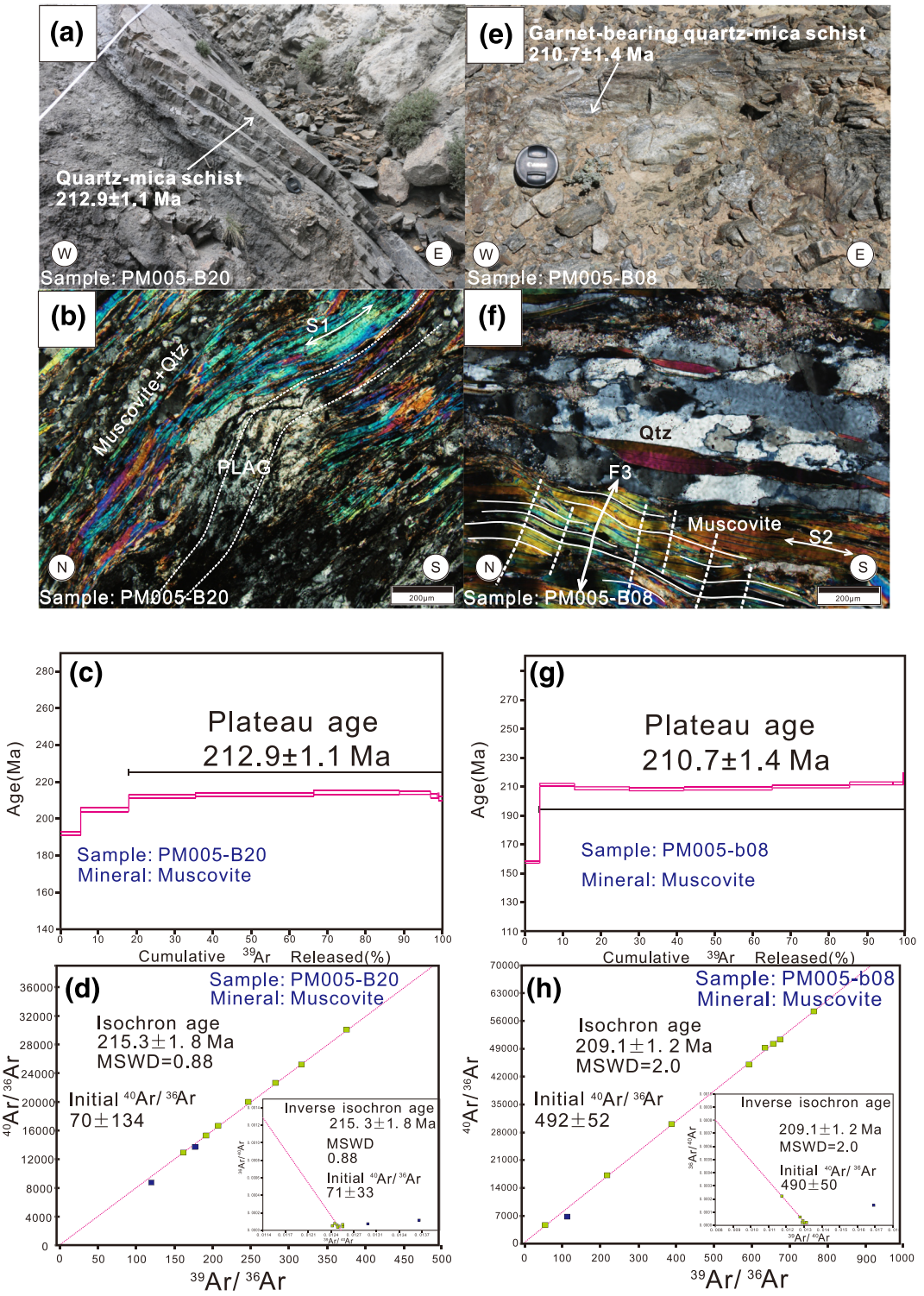

Figure 6. $^{40}Ar/^{39}Ar$ dating. (a) Outcrop where sample PM005-B20 was taken and (b) micrograph of the plagioclase-bearing quartz-mica schist. (c) Age versus cumulative released ^{39}Ar graph, showing a 212.9 ± 1.1 Ma plateau age for the muscovite. (d) The $^{40}Ar/^{36}Ar$ versus $^{39}Ar/^{36}Ar$ graph gives a 215.3 ± 1.8 Ma isochron age. (e) Outcrop where sample PM005-B08 was taken and (f) micrograph of the garnet-bearing quartz-mica schist. (g and h) Muscovite Ar dating resulted in a 210.7 ± 1.4 Ma plateau age and a 209.1 ± 1.2 Ma isochron age.

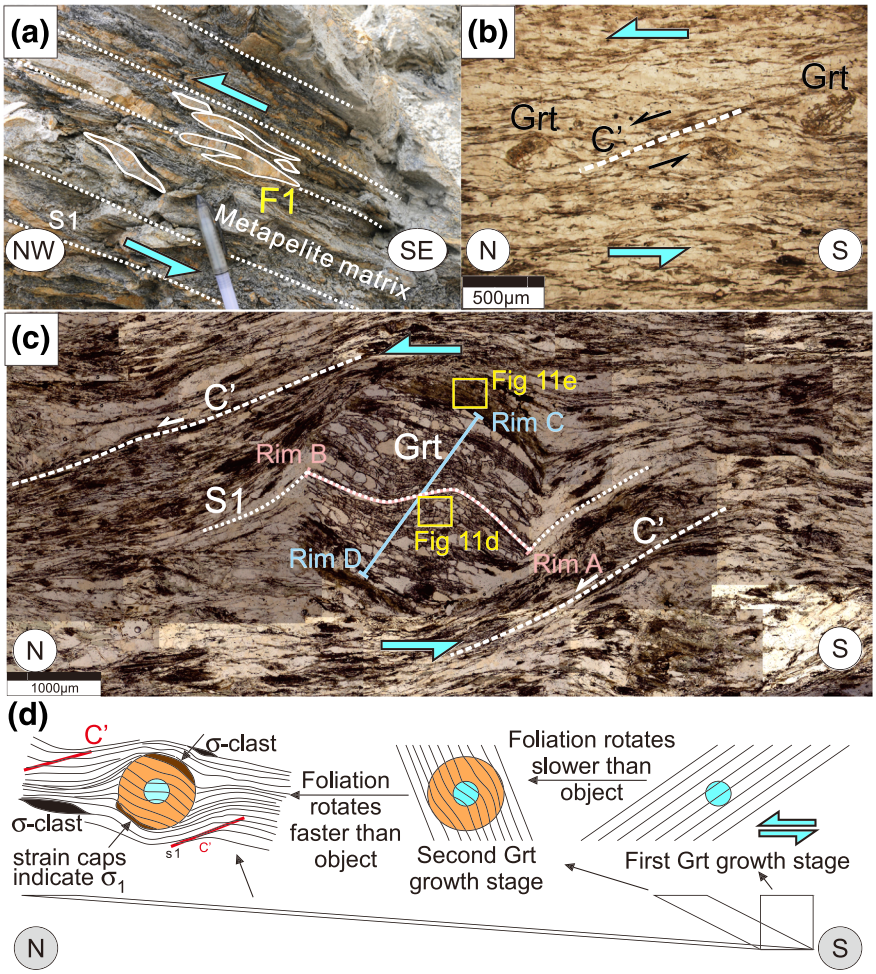

Figure 7. D1 structures in the tectonic (HP) mélange indicate a top-to-the-north sense of shear. (a) Isoclinal rootless fold and asymmetric boudinage. (b) C′-type shear bands and sigma-clasts in phengite schist. (c) The inclusion trail geometry of a garnet in phengite schist shows its syn- to late-D1 growth. The C′ shear band show a top-to-the-north shear sense. The rotation history of the syn-D1 garnet is explained in (d). The line RimA-RimB in the garnet is the location of the chemical profile parallel to the internal fabric in Figure 11b. Line RimC-RimD garnet is the location of chemical profile perpendicular to the internal fabric in Figure 11c. (d) Interpreted evolution in of the syn-D1 garnet and the rotation of the internal fabric relative to the external S1.

3. The stereographic projections of the orientation data of Carboniferous-Permian strata in the Gangma Co areas are placed on the geological maps (Figures 4e and 4g). In addition, the stereographic projection results of the orientation data collected within the mélange are placed on the combined section of I–N (Figures 4f, 5b–5f).
4. All the descriptions and figures (Figures 7, 8, and 9) of structures of the Gangma Co tectonic mélange are organized according to four major deformation stages. These stages of the Gangma Co tectonic mélange and their overprinting relationships are summarized in Figure 10.
5. Shear sense could sometimes already be determined using macroscopic indicators on outcrops. Thin sections were used to further ascertain the shear sense, and to gain information on the metamorphic conditions in relation to deformation stages.

5.1.1. D1 in the Tectonic Mélange

The first recognizable deformation phase, D1, is difficult to discern due to transposition by subsequent deformation phases. D1 is characterized by a layer-parallel foliation (S1), folds, boudins, and quartz veins at all scales.

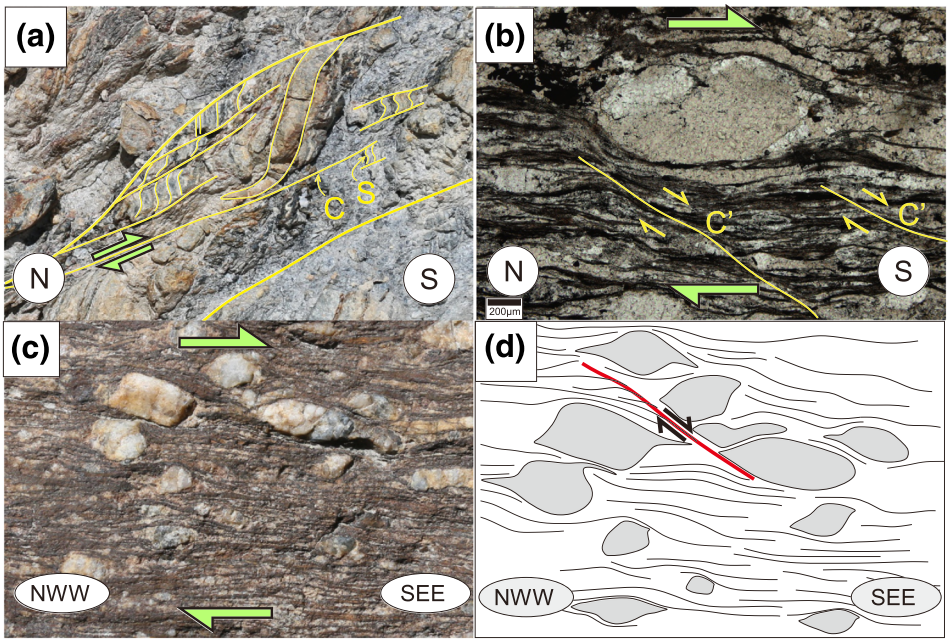

Figure 8. D2 structures in the tectonic (HP) mélange indicate a top-to-the-south sense of shear. (a) Extensional shear bands/crenulations in outcrop. (b) S2-parallel shear zone with a top-to-the-south shear sense indicated by C′ shear bands. (c) A ~40 cm wide S2-parallel shear zone with C′ shear bands and sigmoidal clasts or lenses, with (d) close-up drawing.

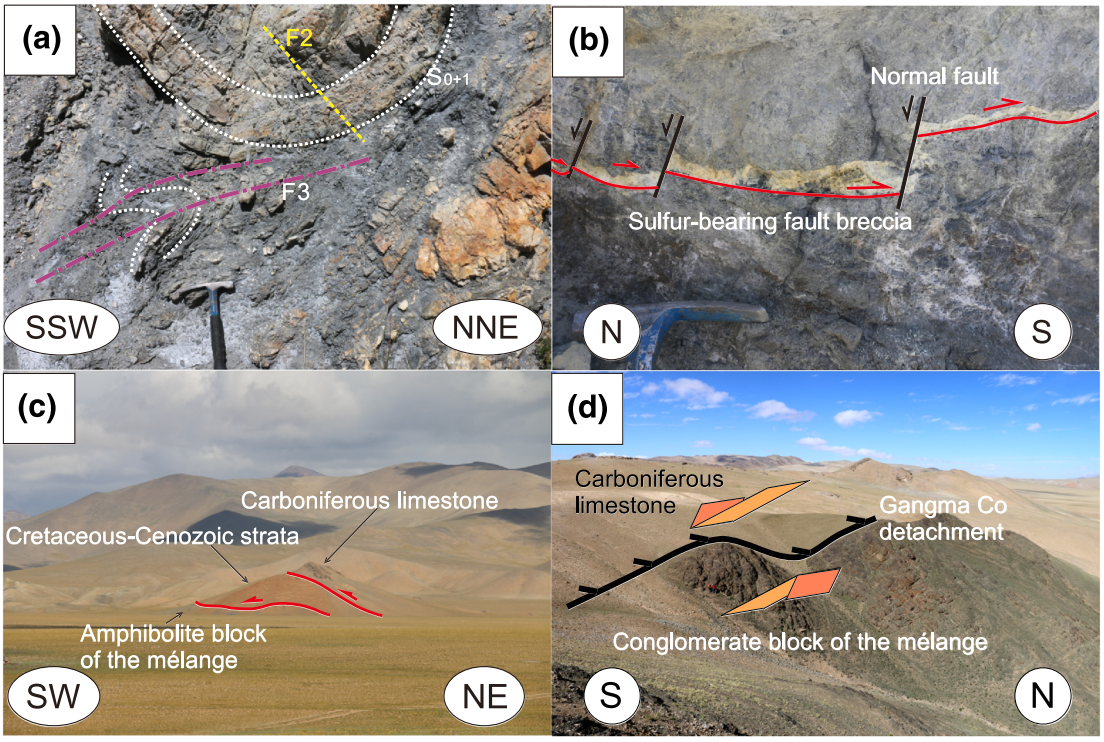

Figure 9. Structures related to D3 and D4 deformation. (a) F3 subhorizontal refolding of F2 folds and S2 foliation. (b) North-dipping D4 thrust fault with sulfur-bearing fault breccia, which is cut by later normal faults. (c) Southward thrusting Carboniferous strata on top of the mélange, with the Cretaceous-Cenozoic strata be placed in between. The location of this contact is marked on Figure 4. (d) The contact of the Carboniferous strata and mélange is mapped by Kapp et al. (2003) as a low-angle detachment fault with a top-to-the-south shear sense. The location of this contact is marked on Figure 4.

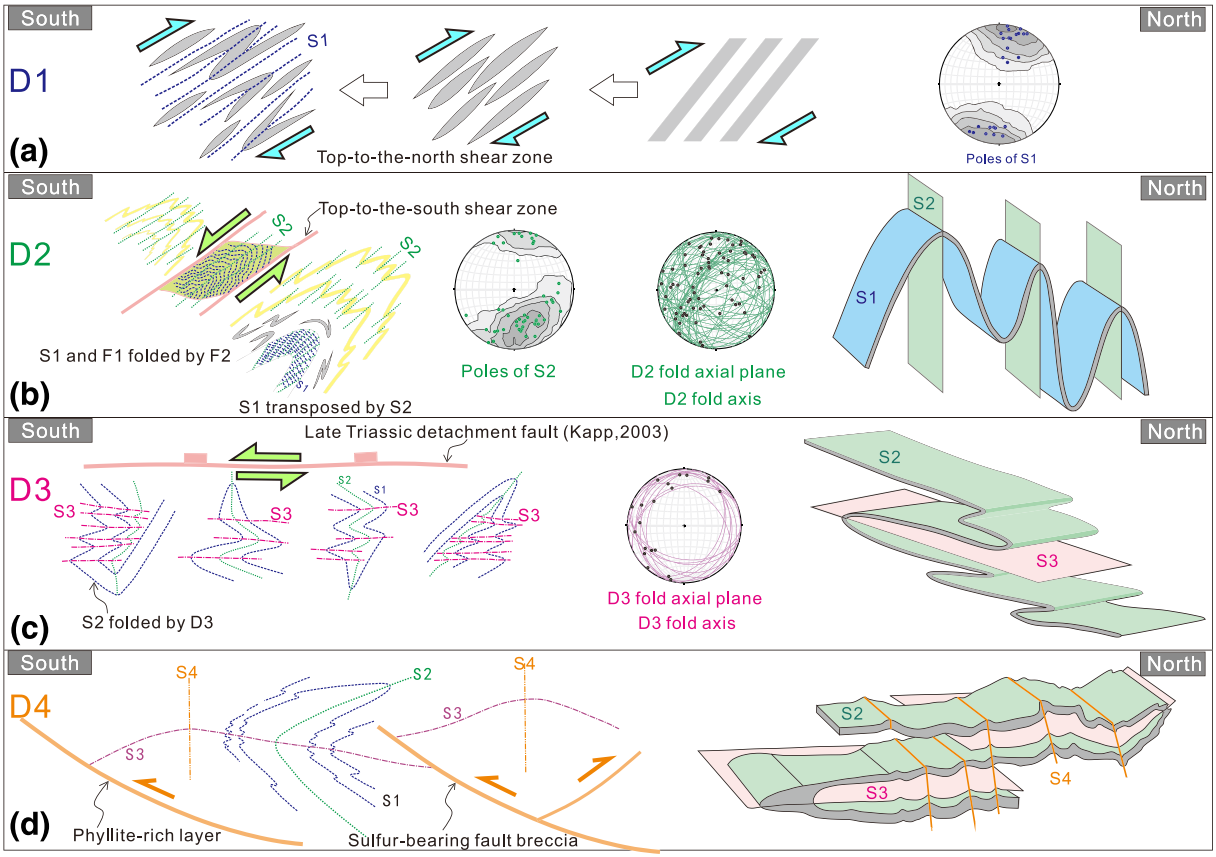

Figure 10. Summary of the deformation history of the mélange. The kinematic information and stereographic projection results of different deformation phase are also shown on the figure. Note that (a) D1 and (b) D2 deformation only occur in tectonic mélange, while D3 deformation (c) affected both the tectonic mélange and sedimentary mélange, as well as the Carboniferous quartzite. This stage is related to the low angle normal detachment fault (Kapp et al., 2003). (d) D4 deformation resulted in a south-vergent fold and thrust belt, affecting all rock units.

F1 folds include passive shear folds and 10 cm-scale intrafolial, isoclinal rootless folds in the mélange matrix (Figure 7a). Compositional layering in quartzofeldspathic (gneiss) schist blocks also sometimes shows isoclinal folds.

A scaly S1 foliation is present in the matrix of the ophiolitic mélange. S1 is mostly parallel to the original lithological layering (S0) that thus together form a composite S0 + 1 foliation (Liang et al., 2017; Figure 7 a), indicative of strong layer-parallel extension or shearing. S1 strikes approximately EW with steep dips (≈60–90°) either to the north or south, due to later folding (Figure 5b). S1 contains a stretching lineation that is defined by the elongation of quartz grains and is highly variable with orientations perpendicular, oblique, or parallel to strike. The S1 foliation wraps around inclusions, lenses, and boudins of relatively competent lithologies (Zhao et al., 2014). Thin quartz sandstone and graywacke units commonly form lenses in the metapelites (Li et al., 2018) and always exhibit mesoscale S-C structures (Kusky & Bradley, 1999). Quartz veins are widespread in the mélange matrix and formed incrementally along the S1 foliation. Asymmetry of folds and sigmoidal shapes of competent lenses indicate a top-to-the-north sense of shear.

Macroscopic D1 deformation structures are extremely rare in the HP mélange and were only found in two outcrops in the more competent lithologies in the form of isoclinal F1 folds. C′-type shear bands and sigma-clasts visible in thin sections of phengite schists show a top-to-the-north sense of shear (Figure 7b). S1 can be found as curved inclusion trails in garnets that are sometimes continuous and connected with the external phengite foliation in the matrix. Figure 7c shows a case where the internal foliation in the core of a garnet has a distinctly different orientation than in the rim. This internal foliation is continuous with the external S1 foliation. This geometry suggests that the garnet grew syn- to late-D1 (Passchier & Trouw, 2005) and that the S1 foliation is associated with peak-pressure conditions.

The internal foliation of the garnet is rotated clockwise relative to the external foliation, which may at first sight be interpreted as indicating top-to-the-south shearing. However, Griera et al. (2011, 2013) and Ran et al. (2018) showed that both the rotation rate of inclusions is progressively reduced and C′-type shear bands develop when the matrix has a mechanical anisotropy. Deflection of the internal foliation shows that the garnet grew in two stages (Figure 7c). This deflection is consistent with an initial foliation that was tilted about 35° relative to the shear plane and top-to-the-north shearing (Figure 7d). At this low angle, a spherical object rotates faster than the foliation. After a shear strain in the order of two, a second growth stage of the garnet occurred. At this stage rotation rate of the foliation is close to its maximum, while that of an object in an anisotropic matrix is expected to have decreased significantly (Griera et al., 2013). Since this point in time, the foliation rotated further toward the shear plane, where it could develop synthetic C′ shear bands. Strain caps furthermore indicate top-to-the-north shear.

5.1.2. D2 in the Tectonic Mélange

D2 deformation structures are the most distinct structures in both the matrix and blocks of the Gangma Co tectonic mélange. These include an S2 foliation that is in axial planar to F2 folds and overprinting S1, F1-folds at all scales of observation, as well as shear zones.

F2 folds are tight to open folds at the cm to >m scale depending on lithology and are characterized by folding of the S1 foliation and/or refolding of F1 isoclinal folds (Li et al., 2018). The associated S2 foliation is a crenulation cleavage formed by microfolding of S1 and the new growth of aligned sericite and biotite (Li et al., 2018; Zhao et al., 2014). Extensional crenulation geometries (Platt & Vissers, 1980) in shear zones extend to the outcrop scale, with narrow shear bands enveloping sigmoidal microlithons in which the curved S0 + 1 foliation is still visible (Figure 8a). The S2-parallel shear bands can develop into up to tens of cm wide shear zones (Figure 8c). The C′ shear bands/zones and sigma clasts or lense geometries in microscale to outcrop scale all indicate a top-to-the-south sense of shear (Figures 8b–8d). This sense of shear is the dominant one in the nonmetamorphic to low metamorphic grade mélange.

The S2 fabric is the main foliation in the HP mélange, where it is formed by microfolding of S1-parallel muscovite and the development of a thin section-scale quartz-rich/poor tectonic layering. In outcrop, this S2 fabric is also defined by muscovite-rich and quartz-rich layers or lenses. Elongate eclogite blocks and pods are aligned with the surrounding S2 foliation.

S2 and axial planes of F2 folds dip about 32–80°, mostly to the NNW. F2 fold axes have highly variable plunge angles and directions (Figure 5d). The shallower dips of S2 (32–45°) are interpreted to be partly reoriented by subsequent D3 folding.

5.2. D3 Deformation Structures

D3 in the ophiolitic and HP-mélange is recognized by refolding of older folds (Figure 9a), but mostly by the reorientation of S1-S2 to shallower dips than their original steep orientation. Axial planes of F3 folds are invariably shallow dipping (7–41°, Figure 5e). The deformation structures indicate that D3 caused vertical shortening and horizontal stretching. A new axial-planar S3 foliation is rarely observed, indicating low metamorphic conditions that inhibit recrystallization or new growth of aligned minerals. Both the sedimentary mélange and Carboniferous quartzites show a layer-parallel foliation, which we interpret as resulting from D3 vertical flattening and potential layer-parallel shearing.

5.3. D4 Deformation Structures

F4 folds are not commonly observed in the tectonic mélange, with only occasional slight refolding of F3 fold limbs. Instead, D4 is characterized by brittle deformation, producing phyllitic fault zones and sulfide-bearing fault breccias (Figure 9b) that cut F3 recumbent folds. Most D4 faults are N-dipping with a S-directed thrust movement. An exception is the S-dipping thrust contact between the HP mélange and the ophiolitic mélange below (Figure 5a). N-directed thrusting (possibly back thrusting) is confirmed by sigma-shaped clasts in the fault zone.

Upright folds of sedimentary layering and layer parallel foliation are found in the sedimentary mélange and Carboniferous rocks (Figures 4c and 4d). Fold axes in these units are mostly WNW-oriented and subhorizontal (Figures 4f and 4g). A steep axial-planar, spaced cleavage developed in the sedimentary mélange, as well as Carboniferous limestones.

Folds and faults together form a fold-and-thrust belt. The south-directed thrusts cut the Cretaceous-Cenozoic sediments that are themselves folded on a large scale (Figure 4b) (Kapp et al., 2000, 2003). Part of the thrusting must therefore have taken place since deposition of these sediments. Zhao et al. (2017) argue for three stages of thrusting in the Rongma area further east in the Qiangtang terrane: Triassic thrusting related to the obduction of the mélange, Jurassic folding, and thrusting related to collision with the Lhasa terrane and finally Late-Cretaceous to Cenozoic folding and thrusting contemporaneous with the formation of intramontane basins. As all these stages involved south-directed thrusting (with potential north-directed back thrusts) it is virtually impossible to assign a thrust to one of the three stages, particularly as faults may be reactivated. We therefore group all brittle thrusting (Figures 9b and 9c) into one D4 event (Figure 10d).

5.4. The Gangma Co Detachment

Kapp et al. (2003) mapped a low-angle fault, the Gangma Co Detachment Fault, that separates the Carboniferous strata from the underlying mélange. According to these authors, the fault is folded and affected by thrusting. The detachment is the clearest in the Shuang Hu area, ca. 365 km east of the study area (Kapp et al., 2003). There S-C mylonites with a top to the SE sense of shear are overlain by chlorite schists and breccia, which is consistent with the proposed core-complex-type detachment. The authors, however, noted that the detachment is not as clear in the Gangma Co area, writing "Additional structural data are necessary to better constrain the kinematics of the detachment fault."

Along most of its trace, the detachment, as mapped by Kapp et al. (2003), coincides with south-directed thrusts, and are depicted as such in Figure 4. The detachment was observed SW of Lake Gangma Co, where Carboniferous limestones overlie breccias/conglomerates that are assigned to the tectonic mélange along a south-dipping fault (Figure 9d). We have not been able to ascertain the kinematics of the fault here. However, we follow Kapp et al. (2003) in recognizing that an originally low-angle normal fault (system) brought metamorphic mélange, including HP rocks, in contact with nongrade to low-grade metamorphic rocks, such as the Carboniferous limestones above. In the study area, the contacts do not show ductile, mylonitic shearing (as in the Shuang Hu area). This puts the activity of the detachment late (D3) in the exhumation history, bringing nonmetamorphic rocks in contact with metamorphic ones.

6. Pressure-Temperature Evolution of D1 Deformation

The phengite schist with syn-D1 garnet (Figure 7d) intercalated between eclogite is selected to determine the pressure-temperature evolution during the D1 deformation stage.

6.1. Petrography and Mineral Chemistry

The minerals were analyzed using a JXA-8100 microprobe in wavelength-dispersive mode with 15 kV acceleration potential and 10 nA beam current at the Institute of Regional Geological Survey of the Hebei Province, China. The phengite schist consists mainly of quartz (q, 45 vol%), phengite (mu, 35%), garnet (grt, 15%), and a small amount of rutile (ru), albite (ab), sphene (sph), chlorite (chl), and calcite.

Three metamorphic stages (M1 to M3) can be distinguished in the evolution of this sample. The mineral assemblage of the M1 stage includes grt + mu + ru + q + law*(epidote + pa). Inclusions of paragonite (pa) and zoisite pseudomorphs after lawsonite (la) (Figure 11d) were found in the core of the garnet porphyroblasts. The mineral assemblage of the M2 stage includes grt + mu + chl + bi + ru + ab + q. The aggregates of biotite (bi) and chlorite mainly occur as later-stage overprinting around garnet and in cracks of garnet. Fine-grained albite and quartz aggregates are also distributed around the garnet (Figure 11e). The mineral assemblage of the M3 stage includes grt + mu + chl + bi + ru + sph + q. In this mineral assemblage, rutile, biotite, and quartz aggregates all exist as inclusions in the sphene (Figure 11f).

The syn-D1 garnets occur as coarse-grained subhedral porphyroblasts with usually frayed boundaries (Figure 7d). The internal fabric of garnet consisting of garnet bands and coarse quartz inclusion trails is obviously curved and continues into the external fabric of the matrix (Figure 7d). Two chemical profiles parallel to and perpendicular to the internal fabric of the garnet were measured (Figure 7d). The chemical profile parallel to the internal fabric is characterized by a core-to-rim increase in both almandine and pyrope contents, which is coupled with a clear decrease in spessartine content, while the grossular content increases gradually and then decreases at the rim. It shows a typical "bell-shaped" profile formed during growth as

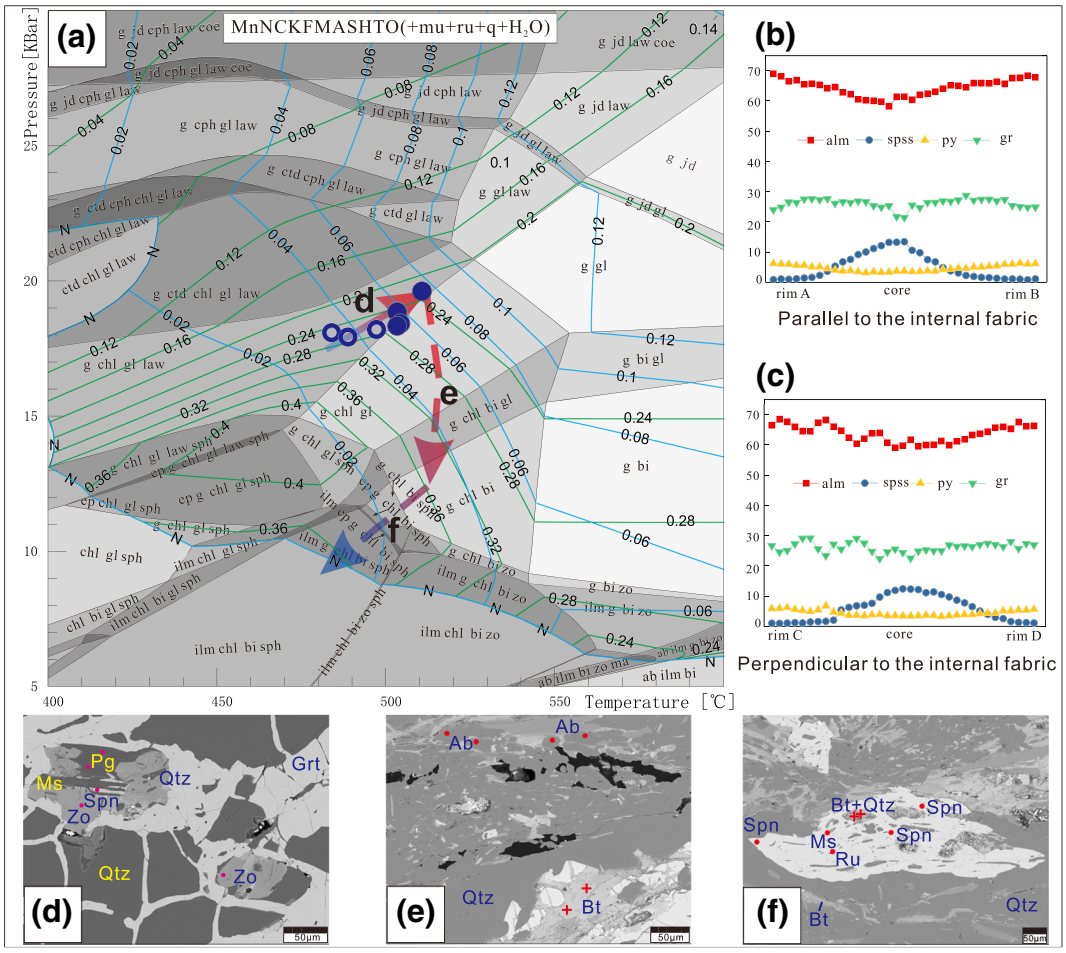

Figure 11. (a) P-T pseudosection for syn-D1 growth garnet-bearing phengite schist in the system MnNCKFMASHTO (+mu + ru + q + H_2O). The bulk composition used for the calculation is Bulk = SI (67.188) AL (14.681) TI (5.922) FE (3.971) CA (0.990) MG (2.004) NA (0.289) MN (0.045) K (4.911) O (177.860) H (100) O (50). Each P-T pseudosection is contoured with isopleths of grossular [=Ca/(Mg + Mn + Ca + Fe2+) × 100] (green solid line) and pyrope [=Mg/(Mg + Mn + Ca + Fe2+) × 100] (blue solid line) contents of garnet. The blue circles correspond to the core composition of garnet, and blue solid circles correspond to the rim composition. Arrows show the resulting PT-path. The first prograde section is based on the chemical profile of the garnet porphyroblast parallel (b) to and perpendicular (c) to the internal fabric (see Figure 7c). (d) Paragonite and zoisite pseudomorphs after lawsonite. (e) Fine-grained biotite and albite on the upper right of the garnet indicate decompression from peak conditions. (f) Sphene and inclusions of muscovite, biotite, and quartz pseudomorphs after rutile indicate further decompression and cooling. Locations of (d) and (e) are marked on Figure 7c.

described by Spear (1995) (Figure 11b). The chemical profile perpendicular to the internal fabric displays a similar zonation, except for the subtly irregular grossular composition (Figure 11c).

6.2. Phase Equilibria Modeling

Phase equilibria modeling was performed for the phengite schist with syn-D1 growth garnet. Because of the retrograde overprinting, the whole-rock data cannot be used to adequately model the phase equilibria observed in this thin section (Wei et al., 2009). Therefore, we synthesized the microprobe mineral data and modal abundances of the M1 stage for the MnNCKFMASHTO model system to estimate the effective bulk-rock composition. Modal abundances were obtained by point-counting. Only half of the modal abundance of the zoned garnet porphyroblast is assumed to be in equilibrium with the matrix minerals (Carson, 1999).

The pseudosection calculation was performed using Theriak-Domino software (de Capitani & Petrakakis, 2010) and the thermodynamics database of Holland and Powell (1998), using the following a–x models: feldspar (Baldwin et al., 2005; Holland & Powell, 2003), epidote (Holland et al., 1998), garnet (White et al., 2005), omphacite (Green et al., 2007), chlorite (Holland et al., 1998), white mica (Holland et al., 1998), talc (Holland

& Powell, 1998), clinoamphibole (Diener et al., 2007). End-members that are treated as pure phases are quartz/coesite, albite, and lawsonite.

The resulting MnNCKFMASHTO P-T pseudosection is presented in Figure 11a. In most mineral assemblages, the isopleths of grossular content show relatively flat slopes with grossular content decreasing as pressure rises, being a good pressure indicator, while the isopleths of pyrope content show steep slopes with pyrope content increasing as temperature rises, being a good temperature indicator (Wei & Clarke, 2011). Thus, the compositional zoning in the syn-D1 growth garnet is plotted on this pseudosection to recover the information of its P-T evolution. The syn-D1 growth garnet preserves clear compositional zoning. The "bell-shaped profiles" in spessartine content that are commonly interpreted to represent growth-dominated zoning (Spear, 1995) are obvious in the chemical profiles, both parallel to or perpendicular to the internal fabric of this garnet (Figures 10b and 10c). All the data plot in the mineral assemblage of grt + chl + gl + law, which is thus located in the glaucophane-lawsonite-bearing eclogite facies. This is in agreement with the presence of lawsonite pseudomorphs and quartz in this garnet. Furthermore, the P-T vector derived by the plot of compositional isopleths of garnet as contours on the P-T pseudosection indicates that this garnet is characteristic of an increase in both pressure (18–19.5 kbar) and temperature (480–510 °C) during its growth (Figure 10a). The presence of lawsonite pseudomorphs consisting of paragonite and zoisite suggest that the prograde path may have occurred within the stability field of garnet, chlorite, glaucophane, and lawsonite, which should be eclogitic facies.

Based on the mineral M2 and M3 mineral assemblages in the phengite schist described above and those of other low-temperature HP rocks in the central Qiangtang terrane (Liu et al., 2011; Wang et al., 2018), a post-peak P-T path with isothermal decompression (M2) and subsequent cooling-decompression (M3) is inferred.

7. Discussion

7.1. Summary of New Observations

This study results in a detailed deformation history and kinematic evolution of the HP-rock bearing CQMB. The oldest D1 structures show ductile shearing with a top-to-the-north shear sense. In the eclogite, D1 shearing occurred under prograde eclogitic facies conditions (T = 480–510 °C, P = 18–19.5 kbar), as indicated by the syn-D1 garnet (Figure 11). Ductile D2 structures show abundant top-to-the-south shear indicators and related folds. Whereas D1 and D2 structures are only found within the tectonic mélange, subsequent deformation stages affected all units in the area. D3 structures are shallowly dipping refolds of previous structures and layer-parallel foliations in the sedimentary mélange and Carboniferous quartzite, indicating vertical shortening and horizontal stretching, which is inferred to have coincided with the top-to-the-south Gangma Co detachment of Kapp et al. (2003). D4 structures include all the later south-vergent thrusts and folds and related backthrusts.

7.2. The Interpretation of HP Rocks Exhumation in Qiangtang Terrane

The formation of HP rocks in the CQMB has been explained with three end-member models (see section 2): (1) the in situ northern subduction model (Li et al., 2009; Liang et al., 2017; Zhang, Cai, et al., 2006), (2) the southward underthrust model (Kapp et al., 2000, 2003; Pullen et al., 2008; Pullen & Kapp, 2014), and (3) the in situ double divergent subduction model (Zhao et al., 2015). However, no direct kinematics evidence has been reported to distinguish between these models.

The observed syn-D1 top-to-the-north sense of shear during progressive eclogitization suggests that the HP-rocks were formed by southward subduction of oceanic crust. Note that the observed tight refolding cannot change this sense of shear (Goscombe & Trouw, 1999). The southward underthrust model, with low-angle subduction of the distal Jinsha oceanic crust (Kapp et al., 2000, 2003; Pullen et al., 2008; Pullen & Kapp, 2014), is consistent with the observed sense of shear. However, as was already pointed out by Zhao et al. (2015), that model is inconsistent with the presence of nonmetamorphosed to low-grade mélange rocks that actually make up most of the mélange in the CQMB. It appears unlikely that these rocks would be the product of pervasive retrogression (Li et al., 2018), as no high-grade relicts have been observed in thin section so far.

A top-to-the-north D1 sense of shear in the HP-rocks is inconsistent with a unidirectional northward subduction underneath the NQT as proposed by Zhang, Cai, et al. (2006), Zhang, Zhang, et al. (2006), Zhang et al. (2007), and Li et al. (2009), leaving the double divergent subduction model with formation of the HP-rocks during southward subduction underneath the SQT as the most viable.

A regional sedimentary hiatus after continuous Carboniferous-Permian deposition in the SQT began in the Late Permian (~260 Ma) (Zhang et al., 2012; Zhao et al., 2015), while the formation of HP-rocks in the CQMB is dated at 233–244 Ma (Li, Zhai, Dong, & Huang, 2006; Pullen et al., 2010; Zhang, Cai, et al., 2006; Zhai et al., 2011), followed by exhumation from 233–220 to ~210 Ma (Dong et al., 2009; Kapp et al., 2003; Li, Zhai, Chen, et al., 2006; Li, Zhai, Dong, & Huang, 2006; Liang et al., 2012; Pullen et al., 2008; Zhai et al., 2009, 2011; Zhang et al., 2010). A short-lived ~20 Ma (from ~260 to ~240 Ma) southward subduction at a few tens of mm/year could have sufficed for up to a few hundred km of subduction, enough to produce HP-rocks, but probably not enough to develop full-fledged arc magmatism, which appears lacking (Zhao et al., 2015).

While the D1 prograde top-to-the-north shear structure was formed by southward subduction, the inverse, the top-to-the-south D2 deformation structures would have formed during exhumation and resulting retrogression. D2 is followed by D3 flattening of older deformation structures in the mélange, but was also experienced by other, non-HP units (Figure 10c). In classical orogenic wedge terminology, such shallow dipping structures tend to be associated with exhumation (Bucher et al., 2003; Chopin et al., 2012; Feehan & Brandon, 1999), especially with doming processes (Rahmati-Ilkhchi et al., 2010; Roger et al., 2015). Extraction of the southward subducted slab from underneath the SQT would in fact constitute a large-scale metamorphic core complex, bound at the top by the top-to-the-south Gangma Co detachment fault, which was originally interpreted as resulting from a very different scenario by (Kapp et al., 2000, 2003; Pullen & Kapp, 2014).

Double subduction underneath both the SQT and NQT results in a convergence in the hinge zones and increasing interaction of the two. As proposed by Zhao et al. (2015), the downward pull of the southern slab would eventually be overridden by the northward pull of the northern slab that is assumed to be longer because of the arc magmatism north of the Longmu Co-Shuanghu suture (Yang et al., 2011). The result would thus be a switch in stress state from horizontal compression (Figure 12a) to vertical compression and horizontal extension (Figure 12b), leading to exhumation and top-to-the-south shearing of the HP-rocks (D2; Figure 13b). The slab was extracted in a metamorphic core complex geometry, where HP-rocks were brought in contact with overlying SQT-margin rocks along the Gangma Co detachment (Figure 13c). HP-rocks underwent a change from dominantly top-to-the-south shearing (D2) to north-south extension and vertical flattening after being brought in contact with overlying nonmetamorphic rocks (D3).

Extraction of the subducted slab would have brought mantle material up in its wake. This is expected to lead to decompressional melting and concomitant magmatic activity. This may explain the voluminous igneous activity recorded in and around the CQMB from ~225 to 210 Ma, coinciding with exhumation from blueschist conditions to the near surface and the Ar/Ar exhumation age acquired from muscovite of eclogitic schists in this study (210 and 212 Ma). However, mantle decompression may not have been sufficient to induce extensive igneous activity during the initial upward movement of oceanic crust. This could explain the preceding period of igneous quiescence when HP rocks exhumed from eclogitic to blueschist level.

The stress state switched back to north-south compression again during final collision of the NQT and SQT, resulting in south-directed thrusting (Figures 12e and 13d). This reactivated the older structures and thrust the structurally deeper mélange onto the upper Carboniferous-Permian strata in places. Extension (D2-D3) and thrusting (D4) have the same sense of shear, except for back thrusts. This makes unraveling the brittle faulting and associated folding difficult, especially since it was later overprinted by shortening associated with the Lhasa-Qiangtang collision.

7.3. The Implication for the HP Rocks Exhumation in Other Orogens

Although the HP rock exhumation models proposed for orogens in the world differ in detail, most researchers agree that they share a number of common upper crustal structures (Beaumont et al., 2009). (1) Exhumation is always accompanied by shear sense inversion (Brun & Faccenna, 2008; Corrie et al., 2012; Favaro et al., 2017; Lee et al., 2000; Rosas et al., 2008; Webb et al., 2007). (2) HP-bearing complexes

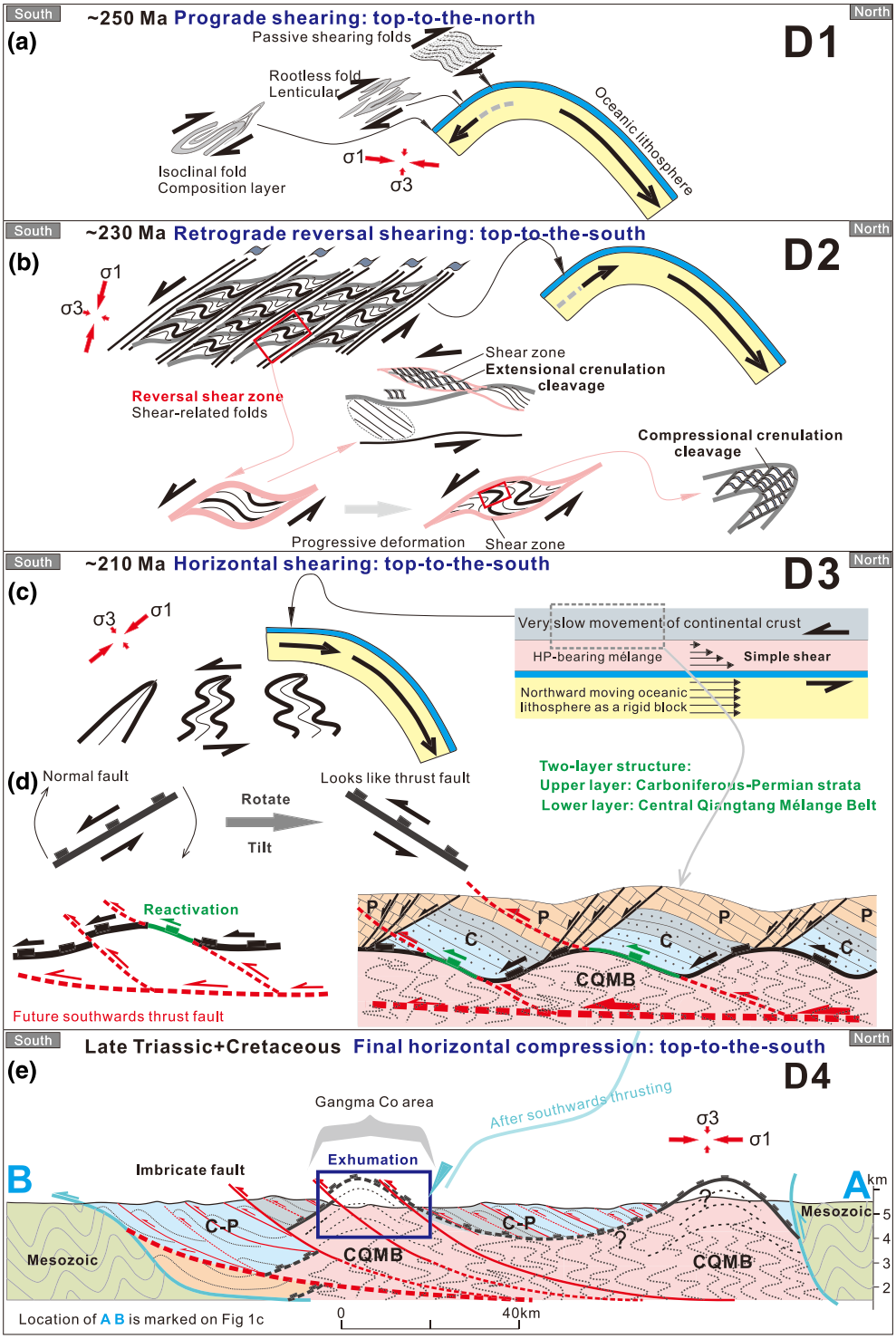

Figure 12. Kinematic and dynamic evolution during the formation and exhumation of HP-bearing mélange. (a) The prograde subduction related shear structures formed by southward subduction. The maximum principal stress σ1 is horizontal, and minimum principal stress σ3 is vertical. (b) Reversal shear zones and related folds during the subduction reversal process of the southern subduction zone. The maximum principal stress σ1 have switched to near vertical. (c) A simple shear setting occurs between the upper crust and lower oceanic lithosphere, driven by the northward moving oceanic plate. (d) Upper Carboniferous-Permian strata are extended and form lithospheric-scale asymmetric boudinage. The core-complex-like dome and related flattening structures of the lower mélange form during this stage. Some segments of the Gangma-Co detachment above the mélange may have tilted to give an apparent thrust movement. (e) Formation of thrust and fold structures during later horizontal compression. The preexisting detachment fault would be reactivated to expose the mélange in the hinterland.

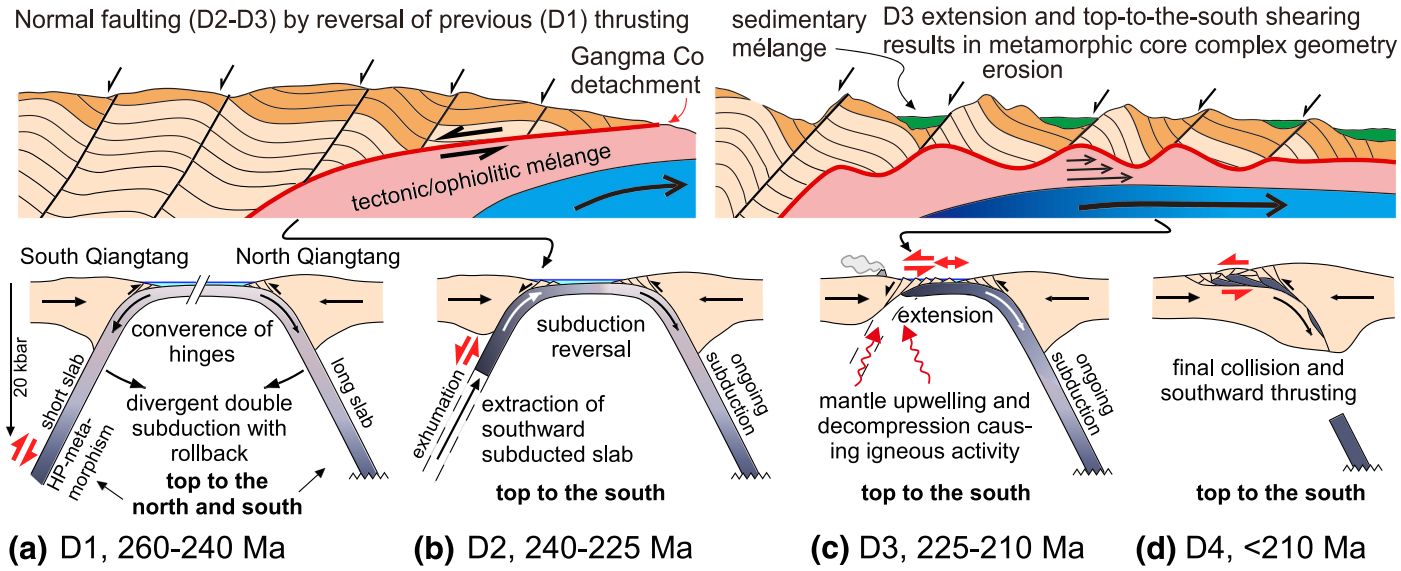

Figure 13. Schematic tectonic evolution of the western part of the central Qiangtang Mélange Belt. (a) Divergent double subduction, which caused to the formation of HP-bearing mélange and related shear structures at the southern suture. (b) Subduction reversal of the southern branch, which caused the shear reversal and HP-bearing mélange exhumation to a shallow level. (c) Northward pull of the northern slab would have produced the core-complex-like dome and two-layer structure. (d) Final collision and later N-S contraction of the North Qiangtang and South Qiangtang cause the exposure of HP-bearing mélange.

typically occupy the core of a structural dome (Ganne et al., 2005; Little et al., 2011; Osozawa & Wakabayashi, 2012), which is usually intruded by granitic plutons (Brun & Faccenna, 2008; Zhao et al., 2012) and (3) is flanked by an accretionary wedge or upper-crustal sedimentary rocks (Faure et al., 2003; Malusà et al., 2011). (4) Many HP-bearing complexes are bounded by shallow-dipping syn-exhumation ductile shear zones above (Beaumont et al., 2009; Platt, 1993). (5) Steep structures in the HP-bearing complex are generally overprinted by shallow-dipping fabrics (Bucher et al., 2003; Chopin et al., 2012). The CQMB exhibits most of these characteristics and is therefore not an exceptional case of HP-rock exhumation.

Our results show that the exhumation-related upper crustal structures and magmatism response can reasonably be explained by subduction reversal, in this case induced by the pull of a second slab in a divergent double subduction system. It may provide a new perspective on the study of exhumation-related upper crustal structures in other orogenic belts in the world, especially where a short-lived double divergent subduction system may have developed. In that case, subduction reversal may be the likely exhumation mechanism of exhumation. To determine this, P-T-D-paths should be extended to P-T-D-sense-of-shear-paths, as was done in this study.

Acknowledgments

All data sets for this research are included in this paper (and its supporting information files) and are available in Bons (2020), "Subduction reversal in a divergent double subduction zone drives the exhumation of southern Qiangtang blueschist-bearing mélange, central Tibet," Mendeley Data (https://doi.org/10.17632/m8g986kwpv). This study was supported by the China Geological Survey (CGS) through grants 1212011221115, DD20190167, and DD20190053. We thank the two reviewers for their supportive and helpful reviews.

Open access funding enabled and organized by Projekt DEAL.

References

Agard, P., Yamato, P., Jolivet, L., & Burov, E. (2009). Exhumation of oceanic blueschists and eclogites in subduction zones: Timing and mechanisms. *Earth-Science Reviews*, *92*(1–2), 53–79. https://doi.org/10.1016/j.earscirev.2008.11.002

Andersen, T. B., Jamtveit, B., Dewey, J. F., & Swensson, E. (1991). Subduction and eduction of continental crust: Major mechanisms during continent-continent collision and orogenic extensional collapse, a model based on the south Norwegian Caledonides. *Terra Nova*, *3*(3), 303–310. https://doi.org/10.1111/j.1365-3121.1991.tb00148.x

Baldwin, J. A., Powell, R., Brown, M., Moraes, R., & Fuck, R. A. (2005). Modelling of mineral equilibria in ultrahigh-temperature metamorphic rocks from the Anápolis-Itauçu Complex, central Brazil. *Journal of Metamorphic Geology*, *23*(7), 511–531. https://doi.org/10.1111/j.1525-1314.2005.00591.x

Baldwin, S. L., Monteleone, B. D., Webb, L. E., Fitzgerald, P. G., Grove, M., & Hill, E. J. (2004). Pliocene eclogite exhumation at plate tectonic rates in eastern Papua New Guinea. *Nature*, *431*(7006), 263–267. https://doi.org/10.1038/nature02846

Beaumont, C., Jamieson, R. A., Butler, J. P., & Warren, C. J. (2009). Crustal structure: A key constraint on the mechanism of ultra-high-pressure rock exhumation. *Earth and Planetary Science Letters*, *287*(1–2), 116–129. https://doi.org/10.1016/j.epsl.2009.08.001

Beaumont, C., Jamieson, R. A., Nguyen, M. H., & Lee, B. (2001). Himalayan tectonics explained by extrusion of a low-viscosity crustal channel coupled to focused surface denudation. *Nature*, *414*(6865), 738–742. https://doi.org/10.1038/414738a

Bottrill, A. D., van Hunen, J., Cuthbert, S. J., Brueckner, H. K., & Allen, M. B. (2014). Plate rotation during continental collision and its relationship with the exhumation of UHP metamorphic terranes: Application to the Norwegian Caledonides. *Geochemistry, Geophysics, Geosystems*, *15*, 1766–1782. https://doi.org/10.1002/2014gc005253

Brueckner, H. K., & Cuthbert, S. J. (2013). Extension, disruption, and translation of an orogenic wedge by exhumation of large ultrahigh-pressure terranes: Examples from the Norwegian Caledonides. *Lithosphere*, *5*(3), 277–289. https://doi.org/10.1130/l256.1

Brueckner, H. K., & van Roermund, H. L. M. (2004). Dunk tectonics: A multiple subduction/eduction model for the evolution of the Scandinavian Caledonides. *Tectonics*, *23*, TC2004. https://doi.org/10.1029/2003tc001502

Brun, J. P., & Faccenna, C. (2008). Exhumation of high-pressure rocks driven by slab rollback. *Earth and Planetary Science Letters*, *272*(1–2), 1–7. https://doi.org/10.1016/j.epsl.2008.02.038

Bucher, S., Schmid, S. M., Bousquet, R., & Fugenschuh, B. (2003). Late-stage deformation in a collisional orogen (Western Alps): Nappe refolding, back-thrusting or normal faulting? *Terra Nova*, *15*(2), 109–117. https://doi.org/10.1046/j.1365-3121.2003.00470.x

Carson, C. J. (1999). Calculated mineral equilibria for eclogites in CaO-Na_2O-FeO-MgO-Al_2O_3-SiO_2-H_2O: Application to the Pouebo Terrane, Pam Peninsula, New Caledonia. *Journal of Metam Geological*, *17*, 9–24.

Chemenda, A. I., Mattauer, M., & Bokun, A. N. (1996). Continental subduction and a mechanism for exhumation of high-pressure metamorphic rocks: New modelling and field data from Oman. *Earth and Planetary Science Letters*, *143*(1–4), 173–182. https://doi.org/10.1016/0012-821x(96)00123-9

Chen, J. W., Li, C., Hu, P. Y., Xie, C. M., Peng, H., & Jiang, Q. Y. (2014). LA-ICP-MS zircon U-Pb age and geochemical characteristics of the granodiorite in the Riwanchaka area, central Qiangtang. *Geological Bulletin of China*, *33*(11), 1750–1758.

Chopin, C. (2003). Ultrahigh-pressure metamorphism: Tracing continental crust into the mantle. *Earth and Planetary Science Letters*, *212*(1–2), 1–14. https://doi.org/10.1016/s0012-821x(03)00261-9

Chopin, F., Schulmann, K., Skrzypek, E., Lehmann, J., Dujardin, J. R., Martelat, J. E., et al. (2012). Crustal influx, indentation, ductile thinning and gravity redistribution in a continental wedge: Building a Moldanubian mantled gneiss dome with underthrust Saxothuringian material (European Variscan belt). *Tectonics*, *31*, TC1013. https://doi.org/10.1029/2011tc002951

Cloos, M. (1982). Flow melanges: Numerical modeling and geologic constraints on their origin in the Franciscan subduction complex, California. *Geological Society of America Bulletin*, *93*(4), 330–345. https://doi.org/10.1130/0016-7606(1982)93<330:Fmnmag>2.0.Co;2

Corrie, S. L., Kohn, M. J., McQuarrie, N., & Long, S. P. (2012). Flattening the Bhutan Himalaya. *Earth and Planetary Science Letters*, *349-350*, 67–74. https://doi.org/10.1016/j.epsl.2012.07.001

Dan, W., Wang, Q., Li, X.-H., Tang, G.-J., Zhang, C., Zhang, X.-Z., & Wang, J. (2019). Low δ18O magmas in the carboniferous intra-oceanic arc, central Tibet: Implications for felsic magma generation and oceanic arc accretion. *Lithos*, *326-327*, 28–38. https://doi.org/10.1016/j.lithos.2018.12.011

Dan, W., Wang, Q., Zhang, X.-Z., Zhang, C., Tang, G.-J., Wang, J., et al. (2018). Magmatic record of Late Devonian arc-continent collision in the northern Qiangtang, Tibet: Implications for the early evolution of East Paleo-Tethys Ocean. *Lithos*, *308-309*, 104–117. https://doi.org/10.1016/j.lithos.2018.03.002

de Capitani, C., & Petrakakis, K. (2010). The computation of equilibrium assemblage diagrams with Theriak/Domino software. *American Mineralogist*, *95*(7), 1006–1016. https://doi.org/10.2138/am.2010.3354

Diener, J. F. A., Powell, R., White, R. W., & Holland, T. J. B. (2007). A new thermodynamic model for clino- and orthoamphiboles in the system Na2O?CaO?FeO?MgO?Al2O3?SiO2?H2O?O. *Journal of Metamorphic Geology*, *25*(6), 631–656. https://doi.org/10.1111/j.1525-1314.2007.00720.x

Dong, Y., Cai, L., Jianrong, S., & ShengYun, W. (2009). Retrograde metamorphism and tectonic emplacement of high pressure metamorphic belt in central Qiangtang Tibet. *Acta Petrologica Sinica*, *25*(9), 2303–2309.

Duretz, T., Gerya, T. V., Kaus, B. J. P., & Andersen, T. B. (2012). Thermomechanical modeling of slab eduction. *Journal of Geophysical Research*, *117*, B08411. https://doi.org/10.1029/2012jb009137

Duretz, T., Gerya, T. V., & May, D. A. (2011). Numerical modelling of spontaneous slab breakoff and subsequent topographic response. *Tectonophysics*, *502*(1–2), 244–256. https://doi.org/10.1016/j.tecto.2010.05.024

Erdman, M. E., & Lee, C.-T. A. (2014). Oceanic- and continental-type metamorphic terranes: Occurrence and exhumation mechanisms. *Earth-Science Reviews*, *139*, 33–46. https://doi.org/10.1016/j.earscirev.2014.08.012

Ernst, W. G., Maruyama, S., & Wallis, S. (1997). Buoyancy-driven, rapid exhumation of ultrahigh-pressure metamorphosed continental crust. *Proceedings of the National Academy of Sciences*, *94*(18), 9532–9537. https://doi.org/10.1073/pnas.94.18.9532

Faure, M., Lin, W., Schärer, U., Shu, L., Sun, Y., & Arnaud, N. (2003). Continental subduction and exhumation of UHP rocks. Structural and geochronological insights from the Dabieshan (East China). *Lithos*, *70*(3), 213–241. https://doi.org/10.1016/S0024-4937(03)00100-2

Favaro, S., Handy, M. R., Scharf, A., & Schuster, R. (2017). Changing patterns of exhumation and denudation in front of an advancing crustal indenter, Tauern Window (Eastern Alps). *Tectonics*, *36*, 1053–1071. https://doi.org/10.1002/2016tc004448

Feehan, J. G., & Brandon, M. T. (1999). Contribution of ductile flow to exhumation of low-temperature, high-pressure metamorphic rocks: San Juan-Cascade nappes, NW Washington State. *Journal of Geophysical Research*, *104*(B5), 10883–10902. https://doi.org/10.1029/1998jb900054

Fu, X. G., Wang, J., Tan, F., Chen, M., Wang, J., Du, B., & Chen, W. (2009). Zircon SHRIMP U-Pb age of volcanic rocks in E'erlongba Formation, eastern part of the Qiangtang basin, Qinghai-Tibet Plateau, China and its geological significance. *Geological Bulletin of China*, *28*(5), 561–567.

Fu, X. G., Wang, J., Tan, F. W., Chen, M., & Chen, W. B. (2010). The Late Triassic rift-related volcanic rocks from eastern Qiangtang, northern Tibet (China): Age and tectonic implications. *Gondwana Research*, *17*(1), 135–144. https://doi.org/10.1016/j.gr.2009.04.010

Ganne, J., Bertrand, J. M., & Fudral, S. (2005). Fold interference pattern at the top of basement domes and apparent vertical extrusion of HP rocks (Ambin and South Vanoise massifs, Western Alps). *Journal of Structural Geology*, *27*(3), 553–570. https://doi.org/10.1016/j.jsg.2004.11.004

Gao, X., JingChao, L., GuoLi, Y., GenHou, W., Xiao, L., YiLong, Z., & Quan, W. (2019). Middle-Late Triassic magmatic records for the accretionary processes of South Qiangtang accretionary terrane: The mafic dykes in Mayigangri-Jiaomuri area, North Tibet. *Acta Petrolei Sinica*, *35*(3), 760–774.

Gerya, T. V., Stöckhert, B., & Perchuk, A. L. (2002). Exhumation of high-pressure metamorphic rocks in a subduction channel: A numerical simulation. *Tectonics*, *21*(6), 1056. https://doi.org/10.1029/2002tc001406

Goscombe, B., & Trouw, R. (1999). The geometry of folded tectonic shear sense indicators. *Journal of Structural Geology*, *21*(1), 123–127. https://doi.org/10.1016/s0191-8141(98)00092-3

Green, E., Holland, T., & Powell, R. (2007). An order-disorder model for omphacitic pyroxenes in the system jadeite-diopside-hedenbergite-acmite, with applications to eclogitic rocks. *American Mineralogist*, *92*(7), 1181–1189. https://doi.org/10.2138/am.2007.2401

Griera, A., Bons, P. D., Jessell, M. W., Lebensohn, R. A., Evans, L., & Gomez-Rivas, E. (2011). Strain localization and porphyroclast rotation. *Geology*, *39*(3), 275–278. https://doi.org/10.1130/g31549.1

Griera, A., Llorens, M.-G., Gomez-Rivas, E., Bons, P. D., Jessell, M. W., Evans, L. A., & Lebensohn, R. (2013). Numerical modelling of porphyroclast and porphyroblast rotation in anisotropic rocks. *Tectonophysics*, *587*, 4–29. https://doi.org/10.1016/j.tecto.2012.10.008

Guillot, S., Hattori, K., Agard, P., Schwartz, S., & Vidal, O. (2009). Exhumation processes in oceanic and continental subduction contexts: A review. *Frontiers of Earth Science*, *175*. https://doi.org/10.1007/978-3-540-87974-9_10

Hacker, B. R., Gerya, T. V., & Gilotti, J. A. (2013). Formation and exhumation of ultrahigh-pressure terranes. *Elements*, *9*(4), 289–293. https://doi.org/10.2113/gselements.9.4.289

Holland, T., Baker, J., & Powell, R. (1998). Mixing properties and activity-composition relationships of chlorites in the system MgO-FeO-Al2O3-SiO2-H2O. *European Journal of Mineralogy*, *395-406*. https://doi.org/10.1127/ejm/10/3/0395

Holland, T., & Powell, R. (1998). An internally consistent thermodynamic data set for phases of petrological interest. *Journal of Metamorphic Geology*, *16*(3), 309–343. https://doi.org/10.1111/j.1525-1314.1998.00140.x

Holland, T., & Powell, R. (2003). Activity–composition relations for phases in petrological calculations: An asymmetric multicomponent formulation. *Contributions to Mineralogy and Petrology*, *145*(4), 492–501. https://doi.org/10.1007/s00410-003-0464-z

Hu, P. Y., Cai, L. I., Yang, H. T., & Zhang, H. B. (2010). Characteristic, zircon dating and tectonic significance of Late Triassic granite in the Guoganjianianshan area, central Qiangtang, Qinghai-Tibet Plateau,China. *Geological Bulletin of China*, *29*(12), 1825–1832.

Hu, P. Y., Li, C., Jie, C., Wang, M., Li, J., & Zhong, L. (2010). Zircon U-Pb dating and Hf-isotope compositions of granodiorite from the Guoganjianian mountain area, central Qiangtang, northern Tibet, China. *Northwest Geology*, *47*.

Jiang, Q. Y., Li, C., Su, L., Hu, P. Y., Xie, C. M., & Wu, H. (2015). Carboniferous arc magmatism in the Qiangtang area, northern Tibet: Zircon U–Pb ages, geochemical and Lu–Hf isotopic characteristics, and tectonic implications. *Journal of Asian Earth Sciences*, *100*, 132–144. https://doi.org/10.1016/j.jseaes.2015.01.012

Kapp, P., Yin, A., Manning, C. E., Harrison, T. M., Taylor, M. H., & Ding, L. (2003). Tectonic evolution of the early Mesozoic blueschist-bearing Qiangtang metamorphic belt, central Tibet. *Tectonics*, *22*(4), 1043. https://doi.org/10.1029/2002tc001383

Kapp, P., Yin, A., Manning, C. E., Murphy, M., Harrison, T. M., Spurlin, M., et al. (2000). Blueschist-bearing metamorphic core complexes in the Qiangtang block reveal deep crustal structure of northern Tibet. *Geology*, *28*(1), 19–22. https://doi.org/10.1130/0091-7613(2000)28<19:Bmccit>2.0.Co;2

Kusky, T. M., & Bradley, D. C. (1999). Kinematic analysis of mélange fabrics: Examples and applications from the McHugh Complex, Kenai Peninsula, Alaska. *Journal of Structural Geology*, *21*(12), 1773–1796. https://doi.org/10.1016/s0191-8141(99)00105-4

Lee, J., Hacker, B. R., Dinklage, W. S., Wang, Y., Gans, P., Calvert, A., et al. (2000). Evolution of the Kangmar Dome, southern Tibet: Structural, petrologic, and thermochronologic constraints. *Tectonics*, *19*(5), 872–895. https://doi.org/10.1029/1999tc001147

Li, C., Zhai, G., Wang, L., Yin, F., & Mao, X. (2009). An important window for understanding the Qinghai–Tibet Plateau—A review on research progress in recent years of Qiangtang area, Tibet, China. *Geological Bulletin of China*, *28*(9), 1169–1177.

Li, C., Zhai, Q., Chen, W., Dong, Y., & Yu, J. (2007). Geochronology evidence of the closure of Longmu Co-Shuanghu suture, Qinghai-Tibet plateau: Ar-Ar and zircon SHRIMP geochronology from ophiolite and rhyolite in Guoganjianian. *Acta Petrologica Sinica*, *23*(5), 911–918.

Li, C., Zhai, Q., Chen, W., Yu, J., Huang, X., & Zhang, Y. (2006). Ar-Ar chronometry of the eclogite from central Qiangtang area, Qinghai-Tibet Plateau. *Acta Petrologica Sinica*, *22*(12), 2843–2849.

Li, C., Zhai, Q., Dong, Y., & Huang, X. (2006). Discovery of eclogite and its geological significance in Qiangtang area, central Tibet. *Chinese Science Bulletin*, *51*(9), 1095–1100. https://doi.org/10.1007/s11434-006-1095-3

Li, D., Wang, G. H., Gao, J., Yuan, G., Zhou, J., Fang, D., et al. (2018). The continental subduction in the evolution of central Qiangtang mélange belt and its tectonic significance. *International Geology Review*, *61*(9), 1143–1170. https://doi.org/10.1080/00206814.2018.1499450

Li, G. M., Li, J.-X., Zhao, J.-X., Qin, K.-Z., Cao, M.-J., & Evans, N. J. (2015). Petrogenesis and tectonic setting of Triassic granitoids in the Qiangtang terrane, central Tibet: Evidence from U–Pb ages, petrochemistry and Sr–Nd–Hf isotopes. *Journal of Asian Earth Sciences*, *105*, 443–455. https://doi.org/10.1016/j.jseaes.2015.02.017

Li, J. C., Zhao, Z., Zheng, Y., Yuan, G., Liang, X., Wang, G., & Liu, X. (2015). The magmatite evidences in southern Qiangtang for Paleo-Tethys Ocean subducting collision: Gangtang-Co granites in Rongma, Tibet. *Acta Petrologica Sinica*, *31*, 2078–2088.

Li, Z. H., Gerya, T. V., & Burg, J.-P. (2010). Influence of tectonic overpressure on P–T paths of HP–UHP rocks in continental collision zones: Thermomechanical modelling. *Journal of Metamorphic Geology*, *28*(3), 227–247. https://doi.org/10.1111/j.1525-1314.2009.00864.x

Liang, X., Wang, G., Yang, B., Ran, H., Zheng, Y., Du, J., & Li, L. (2017). Stepwise exhumation of the Triassic Lanling high-pressure metamorphic belt in central Qiangtang, Tibet: Insights from a coupled study of metamorphism, deformation, and geochronology. *Tectonics*, *36*, 652–670. https://doi.org/10.1002/2016tc004455

Liang, X., Wang, G., Yuan, G., & Liu, Y. (2012). Structural sequence and geochronology of the Qomo Ri accretionary complex, central Qiangtang, Tibet: Implications for the Late Triassic subduction of the Paleo-Tethys Ocean. *Gondwana Research*, *22*(2), 470–481. https://doi.org/10.1016/j.gr.2011.11.012

Liao, J., Malusà, M. G., Zhao, L., Baldwin, S. L., Fitzgerald, P. G., & Gerya, T. (2018). Divergent plate motion drives rapid exhumation of (ultra)high pressure rocks. *Earth and Planetary Science Letters*, *491*, 67–80. https://doi.org/10.1016/j.epsl.2018.03.024

Little, T. A., Hacker, B. R., Gordon, S. M., Baldwin, S. L., Fitzgerald, P. G., Ellis, S., & Korchinski, M. (2011). Diapiric exhumation of Earth's youngest (UHP) eclogites in the gneiss domes of the D'Entrecasteaux Islands, Papua New Guinea. *Tectonophysics*, *510*(1–2), 39–68. https://doi.org/10.1016/j.tecto.2011.06.006

Liu, B. P., & Cui, X. (1983). Discovery of Eurydesma-fauna from Rutog, northwest Xizang (Tibet), and its biogeographic significance. *Earth Science-Journal of Wuhan College of Geology*, *19*, 79–92.

Liu, B. P., Peng, Z., Geng, Q., Zhang, Z., & Guan, J. (2015). LA-ICP-MS zircon U-Pb ages and geochemical features of the granodiorite in Naru area of Shuanghu, Tibet. *Geological Bulletin of China*, *34*(2), 283–291.

Liu, Y., Santosh, M., Zhao, Z. B., Niu, W. C., & Wang, G. H. (2011). Evidence for palaeo-Tethyan oceanic subduction within central Qiangtang, northern Tibet. *Lithos*, *127*(1–2), 39–53. https://doi.org/10.1016/j.lithos.2011.07.023

Liu, Y. M., Xie, C., Li, C., & Li, X. (2017). Structure and development of the Changliangshan ductile shear zone, North Tibet: Implications for the initial closure of the Paleo-Tethys Ocean in the central Qiangtang region. *International Journal of Earth Sciences*, *106*(8), 2945–2962. https://doi.org/10.1007/s00531-017-1478-5

Malusà, M. G., Faccenna, C., Garzanti, E., & Polino, R. (2011). Divergence in subduction zones and exhumation of high pressure rocks (Eocene Western Alps). *Earth and Planetary Science Letters*, *310*(1), 21–32. https://doi.org/10.1016/j.epsl.2011.08.002

Martinez, F., Goodliffe, A. M., & Taylor, B. (2001). Metamorphic core complex formation by density inversion and lower-crust extrusion. *Nature*, *411*(6840), 930–934. https://doi.org/10.1038/35082042

Metcalfe, I. (2013). Gondwana dispersion and Asian accretion: Tectonic and palaeogeographic evolution of eastern Tethys. *Journal of Asian Earth Sciences*, *66*, 1–33. https://doi.org/10.1016/j.jseaes.2012.12.020

Osozawa, S., & Wakabayashi, J. (2012). Exhumation of Triassic HP–LT rocks by upright extrusional domes and overlying detachment faults, Ishigaki-jima, Ryukyu islands. *Journal of Asian Earth Sciences*, *59*, 70–84. https://doi.org/10.1016/j.jseaes.2012.04.001

Pan, G., Ding, J., Yao, D., & Wang, L. (2004). Guidebook of 1:1,500,000 Geologic Map of the Qinghai-Xizang (Tibet) Plateau and Adjacent Areas, Chengdu Cartographic Publishing House, Chengdu, China.

Passchier, C. W., & Trouw, R. A. (2005). *Microtectonics*. Berlin: Springer Science & Business Media.

Petersen, K. D., & Buck, W. R. (2015). Eduction, extension, and exhumation of ultrahigh-pressure rocks in metamorphic core complexes due to subduction initiation. *Geochemistry, Geophysics, Geosystems*, *16*, 2564–2581. https://doi.org/10.1002/2015gc005847

Platt, J. P. (1993). Exhumation of high-pressure rocks: A review of concepts and processes. *Terra Nova*, *5*(2), 119–133. https://doi.org/10.1111/j.1365-3121.1993.tb00237.x

Platt, J. P., & Vissers, R. (1980). Extensional structures in anisotropic rocks. *Journal of Structural Geology*, *2*(4), 397–410. https://doi.org/10.1016/0191-8141(80)90002-4

Pullen, A., & Kapp, P. (2014). Mesozoic tectonic history and lithospheric structure of the Qiangtang terrane: Insights from the Qiangtang metamorphic belt, central Tibet. *Geological Society of America Special Papers*, *507*, 71–87. https://doi.org/10.1130/2014.2507(04)

Pullen, A., Kapp, P., DeCelles, P. G., Gehrels, G. E., & Ding, L. (2011). Cenozoic anatexis and exhumation of Tethyan Sequence rocks in the Xiao Gurla Range, Southwest Tibet. *Tectonophysics*, *501*(1–4), 28–40. https://doi.org/10.1016/j.tecto.2011.01.008

Pullen, A., Kapp, P., Gehrels, G. E., Ding, L., & Zhang, Q. (2010). Metamorphic rocks in central Tibet: Lateral variations and implications for crustal structure. *Geological Society of America Bulletin*, *123*(3–4), 585–600. https://doi.org/10.1130/b30154.1

Pullen, A., Kapp, P., Gehrels, G. E., Vervoort, J. D., & Ding, L. (2008). Triassic continental subduction in central Tibet and Mediterranean-style closure of the Paleo-Tethys Ocean. *Geology*, *36*(5), 351–354. https://doi.org/10.1130/g24435a.1

Rahmati-Ilkhchi, M., Jeřábek, P., Faryad, S. W., & Koyi, H. A. (2010). Mid-Cimmerian, Early Alpine and Late Cenozoic orogenic events in the Shotur Kuh metamorphic complex, Great Kavir block, NE Iran. *Tectonophysics*, *494*(1–2), 101–117. https://doi.org/10.1016/j.tecto.2010.09.005

Ran, H., de Riese, T., Llorens, M. G., Finch, M. A., Evans, L. A., Gomez-Rivas, E., et al. (2018). Time for anisotropy: The significance of mechanical anisotropy for the development of deformation structures. *Journal of Structural Geology*, *125*, 41–47. https://doi.org/10.1016/j.jsg.2018.04.019

Reuber, G., Kaus, B. J. P., Schmalholz, S. M., & White, R. W. (2016). Nonlithostatic pressure during subduction and collision and the formation of (ultra)high-pressure rocks. *Geology*, *44*(5), 343–346. https://doi.org/10.1130/g37595.1

Ring, U., Glodny, J., Will, T., & Thomson, S. (2010). The Hellenic subduction system: High-pressure metamorphism, exhumation, normal faulting, and large-scale extension. *Annual Review of Earth and Planetary Sciences*, *38*(1), 45–76. https://doi.org/10.1146/annurev.earth.050708.170910

Roger, F., Teyssier, C., Respaut, J.-P., Rey, P. F., Jolivet, M., Whitney, D. L., et al. (2015). Timing of formation and exhumation of the Montagne Noire double dome, French Massif Central. *Tectonophysics*, *640-641*, 53–69. https://doi.org/10.1016/j.tecto.2014.12.002

Rosas, F. M., Marques, F. O., Ballèvre, M., & Tassinari, C. (2008). Geodynamic evolution of the SW Variscides: Orogenic collapse shown by new tectonometamorphic and isotopic data from western Ossa-Morena Zone, SW Iberia. *Tectonics*, *27*(6). https://doi.org/10.1029/2008tc002333

Rubatto, D., & Hermann, J. (2001). Exhumation as fast as subduction? *Geology*, *29*(1), 3. https://doi.org/10.1130/0091-7613(2001)029<0003:Eafas>2.0.Co;2

Şengör, A. M. C. (1990). A new model for the late Palaeozoic—Mesozoic tectonic evolution of Iran and implications for Oman. *Geological Society, London, Special Publications*, *49*(1), 797–831. https://doi.org/10.1144/gsl.Sp.1992.049.01.49

Shreve, R. L., & Cloos, M. (1986). Dynamics of sediment subduction, melange formation, and prism accretion. *Journal of Geophysical Research*, *91*(B10), 10229. https://doi.org/10.1029/JB091iB10p10229

Soesoo, A., Bons, P. D., Gray, D. R., & Foster, D. A. (1997). Divergent double subduction: Tectonic and petrologic consequences. *Geology*, *25*(8). https://doi.org/10.1130/0091-7613(1997)025<0755:Ddstap>2.3.Co;2

Spear, F. S. (1995). *Metamorphic phase equilibria and pressure-temperature-time paths*. Washington DC: Short Courses in Geology, Mineralogical Society of America.

Wang, J., Fu, X., Chen, W., Wang, Z., Tan, F., Chen, M., & Zhuo, J. (2008). Chronology and geochemistry of the volcanic rocks in Woruo Mountain region, northern Qiangtang depression: Implications to the Late Triassic volcanic-sedimentary events. *Science in China Series D: Earth Sciences*, *51*(2), 194–205. https://doi.org/10.1007/s11430-008-0010-y

Wang, J., Wang, Z., Chen, W., & Fu, X. (2007). New evidences for the age assignment of the Nadi Kangri Formation in the North Qiangtang depression, northern Tibet, China. *Geological Bulletin of China*, *26*, 404–409.

Wang, S. L., Du, J., Wang, G. H., & Liang, X. (2018). Metamorphic P-T paths of blueschist and lawsonite-bearing phengite schist in Lanling area, central Qiangtang. *Earth Science (in Chinese with English abstract)*, *43*(4), 1237–1252.

Wang, Y., Liang, X., Wang, G., Yuan, G., & Bons, P. D. (2017). Mayer Kangri metamorphic complexes in central Qiangtang (Tibet, western China): Implications for the Triassic–early Jurassic tectonics associated with the Paleo-Tethys Ocean. *International Journal of Earth Sciences.*, *107*(2), 757–776. https://doi.org/10.1007/s00531-017-1526-1

Warren, C. J., Beaumont, C., & Jamieson, R. A. (2008). Modelling tectonic styles and ultra-high pressure (UHP) rock exhumation during the transition from oceanic subduction to continental collision. *Earth and Planetary Science Letters*, *267*(1–2), 129–145. https://doi.org/10.1016/j.epsl.2007.11.025

Webb, A. A. G., Yin, A., Harrison, T. M., Célérier, J., & Burgess, W. P. (2007). The leading edge of the Greater Himalayan Crystalline complex revealed in the NW Indian Himalaya: Implications for the evolution of the Himalayan orogen. *Geology*, *35*(10), 955–958. https://doi.org/10.1130/g23931a.1

Webb, L. E., Baldwin, S. L., Little, T. A., & Fitzgerald, P. G. (2008). Can microplate rotation drive subduction inversion? *Geology*, *36*(10), 823–826. https://doi.org/10.1130/g25134a.1

Wei, C., & Clarke, G. (2011). Calculated phase equilibria for MORB compositions: A reappraisal of the metamorphic evolution of lawsonite eclogite. *Journal of Metamorphic Geology*, *29*(9), 939–952.

Wei, C., Wang, W., Clarke, G. L., Zhang, L., & Song, S. (2009). Metamorphism of high/ultrahigh-pressure Pelitic-Felsic Schist in the South Tianshan Orogen, NW China: Phase Equilibria and P-T Path. *Journal of Petrology*, *50*(10), 1973–1991. https://doi.org/10.1093/petrology/egp064

White, R. W., Pomroy, N. E., & Powell, R. (2005). An in situ metatexite-diatexite transition in upper amphibolite facies rocks from Broken Hill, Australia. *Journal of Metamorphic Geology*, *23*(7), 579–602. https://doi.org/10.1111/j.1525-1314.2005.00597.x

Wu, H., Li, C., Chen, J., & Xie, C. (2016). Late Triassic tectonic framework and evolution of central Qiangtang, Tibet, SW China. *Lithosphere*, *8*(2), 141–149. https://doi.org/10.1130/l468.1

Wu, Y. W., Li, C., Xu, M., Xie, C., & Wang, M. (2017). Zircon U-Pb age, geochemical data: Constraints on the origin and tectonic evolution of the metamafic rocks from Longmuco-Shuanghu-Lancang suture zone, Tibet. *Journal of Earth Science*, *28*(3), 422–432. https://doi.org/10.1007/s12583-017-0730-z

Yang, T. N., Zhang, H. R., Liu, Y. X., Wang, Z. L., Song, Y. C., Yang, Z. S., et al. (2011). Permo-Triassic arc magmatism in central Tibet: Evidence from zircon U-Pb geochronology, Hfisotopes, rare earth elements, and bulk geochemistry. *Chemical Geology*, *284*(3-4), 270–282. https://doi.org/10.1016/j.chemgeo.2011.03.006

Zhai, Q. G., Cai, L. I., & Wang, J. (2009). Petrology, mineralogy and ~(40)Ar/~(39)Ar chronology for Rongma blueschist from central Qiangtang, northern Tibet. *Acta Petrologica Sinica*, *25*(9), 2281–2288.

Zhai, Q. G., Jahn, B. M., Su, L., Wang, J., Mo, X. X., Lee, H. Y., et al. (2013). Triassic arc magmatism in the Qiangtang area, northern Tibet: Zircon U–Pb ages, geochemical and Sr–Nd–Hf isotopic characteristics, and tectonic implications. *Journal of Asian Earth Sciences*, *63*, 162–178. https://doi.org/10.1016/j.jseaes.2012.08.025

Zhai, Q. G., Jahn, B. M., Wang, J., Hu, P. Y., Chung, S. L., Lee, H. Y., et al. (2016). Oldest Paleo-Tethyan ophiolitic mélange in the Tibetan Plateau. *Geological Society of America Bulletin*, *128*(3–4), 355–373. https://doi.org/10.1130/b31296.1

Zhai, Q. G., Jahn, B. M., Wang, J., Su, L., Mo, X. X., Wang, K. L., et al. (2013). The Carboniferous ophiolite in the middle of the Qiangtang terrane, Northern Tibet: SHRIMP U–Pb dating, geochemical and Sr–Nd–Hf isotopic characteristics. *Lithos*, *168-169*, 186–199. https://doi.org/10.1016/j.lithos.2013.02.005

Zhai, Q. G., & Li, C. (2007). Zircon SHRIMP U-Pb age of volcanic rocks in Nadigangri Formation in Juhuashan area, northern part of the Qiangtang basin, Qinghai-Tibet Plateau, China and its geological significance (in chinese). *Acta Geologica Sinica*, *81*(6), 795–800.

Zhai, Q. G., Zhang, R.-Y., Jahn, B.-M., Li, C., Song, S.-G., & Wang, J. (2011). Triassic eclogites from central Qiangtang, northern Tibet, China: Petrology, geochronology and metamorphic P–T path. *Lithos*, *125*(1–2), 173–189. https://doi.org/10.1016/j.lithos.2011.02.004

Zhang, K. J., Cai, J.-X., Zhang, Y.-X., & Zhao, T.-P. (2006). Eclogites from central Qiangtang, northern Tibet (China) and tectonic implications. *Earth and Planetary Science Letters*, *245*(3–4), 722–729. https://doi.org/10.1016/j.epsl.2006.02.025

Zhang, K. J., Tang, X.-C., Wang, Y., & Zhang, Y.-X. (2011). Geochronology, geochemistry, and Nd isotopes of early Mesozoic bimodal volcanism in northern Tibet, western China: Constraints on the exhumation of the central Qiangtang metamorphic belt. *Lithos*, *121*(1–4), 167–175. https://doi.org/10.1016/j.lithos.2010.10.015

Zhang, K. J., Xia, B.-D., Wang, G.-M., Li, Y.-T., & Ye, H.-F. (2004). Early Cretaceous stratigraphy, depositional environments, sandstone provenance, and tectonic setting of central Tibet, western China. *Geological Society of America Bulletin*, *116*(9), 1202–1222. https://doi.org/10.1130/b25388.1

Zhang, K. J., Zhang, Y.-X., Li, B., & Zhong, L.-F. (2007). Nd isotopes of siliciclastic rocks from Tibet, western China: Constraints on provenance and pre-Cenozoic tectonic evolution. *Earth and Planetary Science Letters*, *256*(3–4), 604–616. https://doi.org/10.1016/j.epsl.2007.02.014

Zhang, K. J., Zhang, Y.-X., Li, B., Zhu, Y.-T., & Wei, R.-Z. (2006). The blueschist-bearing Qiangtang metamorphic belt (northern Tibet, China) as an in situ suture zone: Evidence from geochemical comparison with the Jinsa suture. *Geology*, *34*(6), 493–496. https://doi.org/10.1130/g22404.1

Zhang, X. Z., Dong, Y. S., Cai, L. I., Wen, C., Shi, J. R., & Yan, Z. (2010). Identification of the eclogites with different ages and their tectonic significance in central Qiangtang,Tibetan Plateau: Constraints from ~(40)Ar-~(39)Ar geochronology. *Geological Bulletin of China*, *29*(12), 1815–1824.

Zhang, X. Z., YongSheng, D., Cai, L., MingRong, D., Le, Z., & Wang, X. (2014). Tectonic setting and petrogenesis mechanism of Late Triassic magmatism in central Qiangtang, Tibetan Plateau: Take the Xiangtaohu pluton in the Hongjishan region as an example. *Acta Petrologica Sinica*, *30*(2), 547–564.

Zhang, Y. C., Shen, S. Z., Shi, G. R., Wang, Y., Yuan, D. X., & Zhang, Y. J. (2012). Tectonic evolution of the Qiangtang Block, northern Tibet during the Late Cisuralian (Late Early Permian): Evidence from fusuline fossil records. *Palaeogeography, Palaeoclimatology, Palaeoecology*, *350-352*, 139–148. https://doi.org/10.1016/j.palaeo.2012.06.025

Zhang, Y. C., Shi, G. R., & Shen, S.-z. (2013). A review of Permian stratigraphy, palaeobiogeography and palaeogeography of the Qinghai–Tibet Plateau. *Gondwana Research*, *24*(1), 55–76. https://doi.org/10.1016/j.gr.2012.06.010

Zhao, Z. B., Bons, P. D., Stübner, K., Wang, G.-H., & Ehlers, T. A. (2017). Early Cretaceous exhumation of the Qiangtang Terrane during collision with the Lhasa Terrane, Central Tibet. *Terra Nova*, *29*(6), 382–391. https://doi.org/10.1111/ter.12298

Zhao, Z. B., Bons, P. D., Wang, G., Liu, Y., & Zheng, Y. (2014). Origin and pre-Cenozoic evolution of the South Qiangtang basement, Central Tibet. *Tectonophysics*, *623*, 52–66. https://doi.org/10.1016/j.tecto.2014.03.016

Zhao, Z. B., Bons, P. D., Wang, G., Soesoo, A., & Liu, Y. (2015). Tectonic evolution and high-pressure rock exhumation in the Qiangtang terrane, central Tibet. *Solid Earth*, *6*(2), 457–473. https://doi.org/10.5194/se-6-457-2015

Zhao, Z. F., Zheng, Y.-F., Zhang, J., Dai, L.-Q., Li, Q., & Liu, X. (2012). Syn-exhumation magmatism during continental collision: Evidence from alkaline intrusives of Triassic age in the Sulu orogen. *Chemical Geology*, *328*, 70–88. https://doi.org/10.1016/j.chemgeo.2011.11.002

Zhu, D. C., Zhao, Z.-D., Niu, Y., Dilek, Y., Hou, Z.-Q., & Mo, X.-X. (2013). The origin and pre-Cenozoic evolution of the Tibetan Plateau. *Gondwana Research*, *23*(4), 1429–1454. https://doi.org/10.1016/j.gr.2012.02.002